

Accepted Manuscript

Mechanism of Solid-State Clumped Isotope Reordering in Carbonate Minerals from Aragonite Heating Experiments

Sang Chen, Uri Ryb, Alison M. Piasecki, Max K. Lloyd, Michael B. Baker, John M. Eiler

PII: S0016-7037(19)30285-6
DOI: <https://doi.org/10.1016/j.gca.2019.05.018>
Reference: GCA 11244

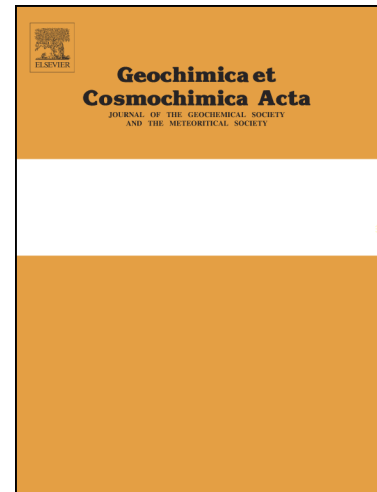
To appear in: *Geochimica et Cosmochimica Acta*

Received Date: 16 October 2018

Accepted Date: 13 May 2019

Please cite this article as: Chen, S., Ryb, U., Piasecki, A.M., Lloyd, M.K., Baker, M.B., Eiler, J.M., Mechanism of Solid-State Clumped Isotope Reordering in Carbonate Minerals from Aragonite Heating Experiments, *Geochimica et Cosmochimica Acta* (2019), doi: <https://doi.org/10.1016/j.gca.2019.05.018>

This is a PDF file of an unedited manuscript that has been accepted for publication. As a service to our customers we are providing this early version of the manuscript. The manuscript will undergo copyediting, typesetting, and review of the resulting proof before it is published in its final form. Please note that during the production process errors may be discovered which could affect the content, and all legal disclaimers that apply to the journal pertain.



1 **Mechanism of Solid-State Clumped Isotope Reordering in Carbonate**
2 **Minerals from Aragonite Heating Experiments**

3
4 *Sang Chen (scchen@caltech.edu)¹, Uri Ryb^{2,1}, Alison M. Piasecki^{1,3}, Max K. Lloyd^{1,4}, Michael B.*
5 *Baker¹, John M. Eiler¹*

6
7 1. Division of Geological and Planetary Sciences, California Institute of Technology, Pasadena,
8 CA 91125, United States

9 2. Fredy and Nadine Herrmann Institute of Earth Sciences, The Hebrew University of Jerusalem,
10 Jerusalem 9190401, Israel

11 3. Department of Earth Science, University of Bergen, Bergen, Norway

12 4. Department of Earth and Planetary Science, University of California, Berkeley, CA 94720,
13 United States

14
15 **Abstract**

16 The clumped isotope compositions of carbonate minerals are subject to alteration at
17 elevated temperatures. Understanding the mechanism of solid-state reordering in carbonate
18 minerals is important in our interpretations of past climates and the thermal history of rocks. The
19 kinetics of solid-state isotope reordering has been previously studied through controlled heating
20 experiments of calcite, dolomite and apatite. Here we further explore this issue through
21 controlled heating experiments on aragonite. We find that Δ_{47} values generally decrease during
22 heating of aragonite, but increase by 0.05–0.15‰ as aragonite starts to transform into calcite. We
23 argue that this finding is consistent with the presence of an intermediate pool of immediately
24 adjacent singly-substituted carbonate ion isotopologues (‘pairs’), which back-react to form
25 clumped isotopologues during aragonite to calcite transformation, revealing the existence of
26 kinetically preferred isotope exchange pathways. Our results reinforce the ‘reaction-diffusion’
27 model as the mechanism for solid-state clumped isotope reordering in carbonate minerals. Our
28 experiments also reveal that the reordering kinetics in aragonite is faster than in calcite and

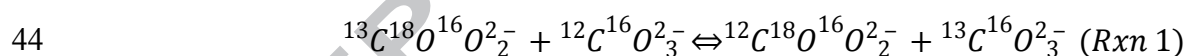
29 dolomite, making its clumped isotope composition highly susceptible to alteration during early
 30 diagenesis, even before conversion to calcite.

31 **Key Words:** aragonite, calcite, clumped isotopes, phase transition, solid-state reordering,
 32 reaction-diffusion model

33

34 **1. Introduction**

35 The carbonate ‘clumped isotope thermometer’ is based on the preferential bonding of ^{13}C
 36 and ^{18}O atoms within the same carbonate ion group at low temperatures, which transitions
 37 toward a more random isotope distribution among carbonate ions at high temperatures (Wang et
 38 al., 2004; Ghosh et al., 2006; Schauble et al., 2006; Eiler, 2011). Carbonate clumped isotope
 39 abundances are reported using the Δ_{47} notation, which is the ratio of the mass 47 isotopologue of
 40 CO_2 ($^{13}\text{C}^{18}\text{O}^{16}\text{O}$) to the mass 44 isotopologue ($^{12}\text{C}^{16}\text{O}_2$) in CO_2 released from a carbonate mineral
 41 by acid digestion, normalized to the ratio expected for a stochastic isotope distribution (Wang et
 42 al., 2004). The thermometer is interpreted to reflect homogeneous isotope exchange equilibrium
 43 between isotopic forms of carbonate ions in the mineral:



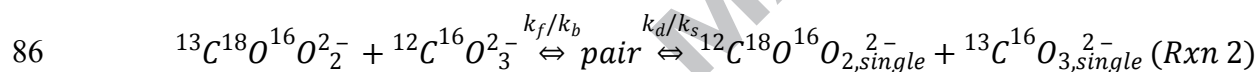
45 The temperature dependent equilibrium constant for this reaction can constrain the temperature
 46 of mineral formation or equilibration, independent of the carbon and/or oxygen isotope
 47 composition of the fluid from which the mineral grew, and of the mineral itself (Eiler, 2007;
 48 Eiler, 2011). This quality makes this proxy useful for reconstructing Earth-surface temperatures
 49 for geological times and locations where the ^{18}O content of the water is not well known (e.g.,
 50 Thiagarajan et al., 2014; Tripathi et al., 2014; Rodriguez-Sanz et al., 2017; Henkes et al., 2018).
 51 Carbonate clumped isotope thermometry has also been used to infer temperatures of processes

52 that occur in the shallow crust such as diagenesis (Dennis & Schrag, 2010; Huntington et al.,
53 2011; Cummins et al., 2014; Winkelstern & Lohman, 2016; Ryb & Eiler, 2018) and
54 metamorphism (Ferry et al., 2011; Ryb et al., 2017; Lloyd et al. 2017).

55 The application of carbonate clumped isotope thermometry to the reconstruction of
56 climate, water $\delta^{18}\text{O}$ values, or the thermal histories of rocks is complicated by the alteration of
57 Δ_{47} values at elevated burial temperatures through solid-state reordering of C–O bonds (Passey &
58 Henkes, 2012; Henkes et al., 2014; Stolper & Eiler 2015; Lloyd et al., 2017; Shenton et al., 2015;
59 Gallagher et al., 2017; Lacroix & Niemi, 2019; Ryb et al., 2017; Ingalls, 2019). Previous studies
60 have used controlled heating experiments to constrain the kinetics of solid-state isotope
61 reordering of calcite (Passey & Henkes, 2012; Henkes, et al., 2014; Stolper & Eiler, 2015;
62 Brenner et al., 2018), apatite (Stolper & Eiler, 2015) and dolomite (Lloyd et al., 2018). In these
63 experiments, aliquots of the mineral of interest were held at a constant temperature for different
64 amounts of time to create a time series over which the mineral Δ_{47} values could be observed to
65 gradually approach equilibrium appropriate for that temperature. The rate of change of Δ_{47} values
66 observed in such experiments constrains the kinetics of isotopic re-distribution among carbonate
67 ions in the mineral lattice.

68 A key finding of these previous experiments is that solid-state alteration of Δ_{47} values in
69 calcite, apatite, and dolomite all follow non-first-order kinetics. This finding has been interpreted
70 as evidence that isotopic reordering is a two-stage process involving two mechanisms with
71 different rate laws. Early in each set of time-series experiments, the rate of change of Δ_{47} values
72 is dominated by a relatively fast process, which sharply transitions to a slower process that
73 controls the remainder of the time series. Passey & Henkes (2012) attributed the initial rapid
74 decrease in Δ_{47} in calcite to rapid diffusion facilitated by initially abundant lattice defects, and

75 suggested the transition to slower kinetics reflects annealing of those defects, reducing their
 76 abundance and therefore the overall rate of isotopic re-equilibration. Stolper & Eiler (2015)
 77 proposed an alternative reaction-diffusion model to explain the two stages of calcite reordering.
 78 This model introduced the concept of ‘pairs’ and ‘singletons’. Whereas a ‘clump’ is a carbonate
 79 group that contains both ^{13}C and ^{18}O , a ‘pair’ is a set of two adjacent carbonate groups, one of
 80 which contains ^{13}C and the other of which contains ^{18}O , while a ‘singleton’ is any carbonate
 81 group that contains either a single ^{13}C or a single ^{18}O , and has as immediate neighbors only
 82 carbonate ion units that lack ^{13}C and ^{18}O (i.e., they are all $^{12}\text{C}^{16}\text{O}_3^{2-}$). Stolper and Eiler (2015)
 83 suggested that clumped isotope evolution reflects rapid exchange between ‘clumps’ and ‘pairs’
 84 coupled with slow diffusion-controlled separation of ‘pairs’ into isolated ‘singletons’ (Figure 1a).
 85 In this case, the reordering reaction is described by the equation:



87 where k_f is the forward rate of transformation of a clump and neighboring unsubstituted
 88 carbonate ion into a pair, k_b is the rate of back reaction of a pair to form a clump, k_d is the
 89 diffusion-controlled rate of separation of pairs to form singletons, and k_s is the rate of diffusion
 90 for singletons to remake pairs.

91 The presence of the intermediate pool of pairs can explain the two stages of clumped
 92 isotope reordering as follows (Stolper and Eiler, 2015): The first stage of rapid reaction is
 93 dominated by the formation of pairs from clumps through isotope exchange of immediately
 94 adjacent neighbors, while the second stage is dominated by diffusion in the crystal lattice.
 95 Because the second stage is slower than the first, the region surrounding initial clumps become
 96 saturated with pairs of singly-substituted carbonate ion units that have not yet diffused away
 97 from each other; back reaction of this saturated pool of pairs is what buffers the decrease in the

98 Δ_{47} value during the slower, diffusion-limited stage of the time series. Stolper and Eiler (2015)
99 did not offer an atomistic explanation for why the transition from clump to pair is faster than the
100 separation of pairs — intuition might predict these should have the same rate, as both types of
101 reactions involve migration of ^{18}O (and perhaps ^{13}C) from one carbonate ion unit to another. This
102 unresolved aspect of the reaction-diffusion model is one of the inspirations for the present study.

103 While both the defect-annealing and reaction-diffusion models have been successfully
104 applied to natural samples (Henkes et al., 2014; Shenton et al., 2015; Lloyd et al., 2017; Ryb et
105 al., 2017, Ingalls, 2019), it has been argued that the reaction-diffusion model is favored by the
106 observation that the kinetics of isotopic reordering in optical calcite, brachiopods, and deformed
107 and undeformed natural marbles are indistinguishable from one another (the idea being that these
108 diverse materials might be expected to differ in their initial defect populations; Stolper & Eiler,
109 2015; Ryb et al., 2017; Lloyd et al., 2018). Nevertheless, there is a strong motivation to establish
110 which of these two interpretations (or perhaps some other not yet proposed) is correct. And, if
111 the reaction-diffusion model is correct, we still must understand why it is that an initial exchange
112 between two adjacent carbonate ion groups is significantly faster than subsequent, but otherwise
113 generally similar exchanges. The answers to these questions will dictate how carbonate clumped
114 isotope measurements are used to reconstruct temperature-time histories of rocks that have been
115 heated during protracted burial in sedimentary basins, and may inspire new tools based on the
116 physical processes that control this phenomenon.

117 In this study, we re-examine this problem through observations of the kinetics of Δ_{47}
118 changes when aragonite is exposed to elevated temperatures, at either high pressure where
119 aragonite remains stable during heating, or at low pressure where it transforms into calcite over
120 the time scales of our heating experiments. This work was initiated to obtain constraints on the

121 susceptibility of aragonite to clumped-isotope reordering at shallow crustal conditions. However,
122 our initial experimental results made it clear that this process provided an unexpected window on
123 the atomistic mechanisms of the general phenomenon of clumped isotope reordering.

124 Aragonite is a polymorph of calcium carbonate that is common in nature, despite the fact
125 that it is thermodynamically unstable at Earth surface conditions and readily transforms into
126 calcite through heating or dissolution-precipitation reactions (Jamieson, 1953; Bischoff, 1969;
127 Carlson, 1980; Budd, 1988). Clumped isotope compositions of aragonite follow the same
128 temperature vs. Δ_{47} calibration curve as other carbonate minerals (Ghosh et al., 2006;
129 Thiagarajan et al., 2011; Bonifacie et al., 2017). Clumped isotope compositions of fossil
130 aragonite have been used in paleoclimate reconstructions of the recent ice age (Thiagarajan et al.,
131 2014) and deeper times of the Phanerozoic (Dennis et al., 2013). Given its thermodynamic
132 instability, it has generally been assumed that aragonite found in nature has been unaltered in its
133 elemental and isotopic compositions. Recently, it has been shown in laboratory experiments and
134 natural speleothems that the carbon, oxygen, and clumped isotope compositions can all be
135 altered during the aragonite to calcite phase transition (Zhang et al., 2014; Staudigel & Swart,
136 2016). In particular, Staudigel & Swart (2016) observed complicated clumped isotope reordering
137 patterns in aragonite heating experiments over a range of temperatures (125–425°C), including
138 unexpected increases in Δ_{47} values during the heating process in certain experiments. These
139 increases in Δ_{47} values are, however, not consistently observed in all their experiments, and are
140 statistically indistinguishable from the previous time step in many cases. The authors noted these
141 complexities but described aragonite reordering with a first order kinetic model. Staudigel &
142 Swart (2016) also noticed that aragonite reordering initiates at lower temperatures than does
143 calcite. However, a systematic decreasing trend in the bulk isotope composition (2.5‰ in $\delta^{18}\text{O}$

144 and 1.5‰ in $\delta^{13}\text{C}$) with time was observed in these experiments, suggesting a possible influence
145 of open system exchange that would complicate the interpretation of these data as simply
146 reflecting the solid-state reordering process.

147 We present new aragonite reordering experiments that reproduce and extend the
148 previously observed complex clumped isotope reordering patterns, and we explain these findings
149 as natural consequences of the reaction-diffusion model in a system undergoing a phase
150 transition. We then test this hypothesis further through experiments in which we manipulate the
151 distributions of clumped, pair, and singleton carbonate groups by preliminary thermal treatments
152 to aragonite and calcite, and then observe the effect of those treatments on the solid-state
153 reordering kinetics of both phases in a second heating experiment (Figure 1b,c). We summarize
154 our hypothesis and experimental tests in the reaction-diffusion framework with a fluid-flow
155 analogy in Figure 1, which are detailed in the following sections. Our experimental results
156 suggest the presence of an intermediate pool of pairs in both aragonite and calcite, re-enforcing
157 the reaction-diffusion model of clumped isotope reordering.

158

159 **2. Materials and Methods**

160 *2.1 Aragonite Samples*

161 The aragonite used in our experiments was obtained from Tazouta, Sefrou Province, Fès-
162 Boulemane, Morocco. It is a fist-sized aggregate of faceted intergrown crystals that are 0.5–1 cm
163 in size. The sample was chosen due to its size, visual homogeneity and low-temperature origin.
164 Replicate analysis ($n = 21$) of the bulk and clumped isotope composition of the aragonite yields a
165 $\delta^{13}\text{C}$ value of $7.53 \pm 0.17\text{‰}$ (VPDB), a $\delta^{18}\text{O}$ value of $-7.49 \pm 0.19\text{‰}$ (VPDB), and a Δ_{47} value of
166 $0.757 \pm 0.028\text{‰}$ (means and aliquot-to-aliquot standard deviations; all reported Δ_{47} values are

167 given in the absolute reference frame following Dennis et al., 2011). The Δ_{47} value corresponds
168 to a formation temperature of $16\pm 5^\circ\text{C}$ (Dennis et al., 2011). The reported standard deviations of
169 bulk and clumped isotope compositions are higher than the long-term reproducibility of
170 carbonate standards at Caltech (0.03‰ for $\delta^{13}\text{C}$, 0.08‰ for $\delta^{18}\text{O}$, 0.02‰ for Δ_{47}), and suggest
171 some natural heterogeneity within our sample. In interpreting our experiment results, we
172 consider a measured isotope composition of a sample significantly different from others only
173 when these differences exceed the internal variabilities in the starting materials.

174

175 *2.2 Aragonite Reordering Experiments*

176 The aragonite crystals were coarsely crushed into ~ 10 mg fragments (each ~ 1 – 2 mm
177 across). The crystals were not further reduced in grain size because we wished to minimize the
178 surface area and therefore any effects of adsorbed water or other surface chemistry.
179 Approximately 20 mg of aragonite fragments were sealed in $\frac{1}{4}$ " quartz or Pyrex® tubes with 6.6
180 kPa isotopically distinct CO_2 gas ($\delta^{13}\text{C} = -11\text{‰}$, $\delta^{18}\text{O} = +16\text{‰}$, VPDB) in the headspace. The
181 CO_2 gas was cryogenically purified with a dry ice-ethanol mixture to remove water vapor. The
182 experiments were carried out under CO_2 atmosphere to minimize decarbonation of the aragonite,
183 as well as to detect whether open-system isotope exchange reactions had occurred. The tubes
184 containing aragonite and CO_2 were put into a box furnace held at one of several prescribed
185 temperatures (200–500°C). For each temperature, different aragonite samples were heated for
186 different lengths of time to create a time series of clumped isotope reordering. After heating, we
187 weighed each sample and determined the fractions of aragonite and calcite in the samples by X-
188 ray diffraction (XRD) or Raman spectroscopy before isotope compositions were measured. For
189 most samples, the weight loss is < 0.3 mg before and after heating, and the bulk isotope

190 compositions are within the initial heterogeneities of the starting material, consistent with no
191 decarbonation or open-system exchange (Table 1, Figure 2c,f). In three of the heating
192 experiments, the aragonite was run in unsealed tubes and thus was exposed to the ambient
193 atmosphere (Table 1). As with the sealed tube experiments, no significant decarbonation or open
194 system exchange was observed for these three experiments. The aragonite to calcite phase
195 transition was faster when exposed to the ambient atmosphere (Figure 2b,e), but the clumped
196 isotope reordering pattern was similar to the experiments with sealed tubes.

197

198 *2.3 High-Pressure Aragonite Experiment*

199 For this experiment, we used a cylinder cored from a large crystal that comprised a
200 portion of our aragonite sample. The core (260 mg) was loaded into a 0.2" (outer diameter) Au
201 capsule welded at both ends (for the second weld, the capsule was partially immersed in a water
202 bath to minimize any heating of the aragonite). The capsule was run in a 1/2" piston cylinder
203 pressure vessel using an assembly that consisted of inner pieces of MgO (dried at 1000°C for ~8
204 hours), a straight-walled graphite furnace, and an outer sleeve of calcium fluoride. Temperature
205 was monitored and controlled to within 1°C of the set point using a W₃Re/W₂₅Re thermocouple
206 (care was taken to avoid thermocouple oxidation by bleeding N₂ gas into the slot in the
207 thermocouple plate). Run conditions were 1.7 GPa and 600°C and the sample was quenched after
208 10 days. Based on thermocouple output as a function of time, the sample cooled to room
209 temperature in ~30 s. The experiment was designed to equilibrate the clumped isotope
210 composition (and potentially the concentration of pairs) at high temperature while maintaining
211 aragonite in its stability field. The *P-T* conditions of the experiment were well within the
212 aragonite field based on the CaCO₃ *P-T* phase relations compiled by Carlson (1980), and Raman

213 spectroscopy showed that the post-run material was, indeed, aragonite (Figure 3c). Next, an
214 aliquot of this *P-T*-treated aragonite was measured for bulk and clumped isotope composition,
215 while other fragments went through a reordering experiment at 350°C at ambient pressure in a
216 CO₂ atmosphere (see Section 2.2) before isotopic analysis. A 350°C reordering experiment using
217 untreated fragments of the aragonite was carried out in parallel for direct comparison.

218

219 *2.4 Two-Step Calcite Heating Experiment*

220 The two-step calcite heating experiment was designed to test if the complex clumped
221 isotope reordering behavior in aragonite, in particular increases in Δ_{47} during heating, can occur
222 in calcite. An optical calcite (catalog # N21-1) was selected from the Caltech mineral collection
223 for its size, clarity, lack of visible defects or inclusions, and its relatively low-temperature origin.
224 Bulk and clumped isotope analyses ($n = 17$) yield a $\delta^{13}\text{C}$ value of $-1.55 \pm 0.45\text{‰}$ (VPDB), a $\delta^{18}\text{O}$
225 value of $-16.96 \pm 0.30\text{‰}$ (VPDB) and a Δ_{47} value of $0.586 \pm 0.006\text{‰}$, which corresponds to a
226 temperature of $63 \pm 3^\circ\text{C}$ (Bonifacie et al., 2017). While the bulk isotope compositions of this
227 calcite show substantial heterogeneity, the clumped isotope composition is relatively
228 homogeneous. The sample was crushed into 10–30 mg fragments and sealed in quartz tubes with
229 6.6 kPa purified CO₂ gas that is isotopically distinct ($\delta^{13}\text{C} = -11\text{‰}$, $\delta^{18}\text{O} = +16\text{‰}$, VPDB) in the
230 headspace. The tubes were initially heated at 450°C for 5 hours, and cooled quickly to room
231 temperature (within ~2 minutes) using a compressed air duster. In the second step of this
232 experiment, the pretreated samples from the first step were heated at 500°C for different time
233 intervals. We repeated this experiment twice to generate a replicate set of samples.

234

235 *2.5 Mineralogy*

236 In order to determine the extent to which aragonite transformed to calcite during the low-
237 pressure, high-temperature experiments, samples were analyzed post-run by XRD or Raman
238 spectroscopy. XRD measurements were performed with a Bruker D2 Phaser benchtop instrument
239 (Cu K_{α} source) at Caltech. Relative peak areas at specific 2θ angles (30° for calcite, 46° for
240 aragonite) were compared to determine the proportions of aragonite and calcite in the samples,
241 using an approach similar to Dickinson & McGrath (2001). Relative peak areas were converted
242 to mass fractions with a calibration curve generated from powder mixtures of pure aragonite and
243 calcite. The detection limit of the method is approximately 1% for calcite and 5% for aragonite.

244 The Raman measurements were performed on a Renishaw M1000 Micro Raman
245 Spectrometer at Caltech. The system uses a solid-state 514.3 nm laser with 100 mW beam power,
246 and the measurements were done with 10% power at 5x magnification (~ 2 mW on sample) to
247 minimize sample damage and maximize the covered area. Multiple spots ($n = 5-10$) were
248 measured for each sample to get an average spectrum. Following Dickinson & McGrath (2001),
249 the relative proportions of aragonite and calcite were determined using the scattering peaks for
250 the carbonate ion planar bending mode (704 cm^{-1} for aragonite, 713 cm^{-1} for calcite). Relative
251 peak areas were converted to mass fractions with a calibration constructed from powder mixtures
252 of pure aragonite and calcite (Figure 3). The peak areas scale close to 1:1 with mass fractions in
253 the calibration standards. The Raman method was used for most samples because it requires less
254 material than the XRD method we employed, and limited amounts of sample were recovered
255 from each experiment (especially the high-pressure experiment described in Section 2.3). We
256 also viewed the Raman measurement as more robust because of the greater linearity of its
257 calibration trend.

258

259 2.6 Stable Isotope Measurements

260 The bulk and clumped isotope compositions of the samples were measured using a
261 Thermo MAT253 isotope ratio mass spectrometer at Caltech. Sample preparation and analysis
262 procedures have been previously described in detail (Ghosh et al., 2006; Guo et al., 2009;
263 Huntington et al., 2009; Passey et al., 2010). In brief, samples (~10 mg) were digested in
264 phosphoric acid at 90°C. Evolved CO₂ gas was purified cryogenically and went through a
265 Porapak Q (50/80 mesh) GC column held at -20°C, and then measured against a reference CO₂
266 gas. The measurements were standardized to heated (1000°C) and water-equilibrated (25°C) CO₂
267 gases, and in-house carbonate standards. In the calculation of bulk and clumped isotope
268 compositions, we used the ¹⁷O/¹⁶O, ¹⁸O/¹⁶O ratios for VSMOW and the ¹³C/¹²C ratio for VPDB
269 suggested by Brand et al. (2010), which were found to minimize inter- and intra-laboratory
270 discrepancies in reported Δ₄₇ values (Schauer et al., 2016; Daëron et al., 2016). Measurements
271 and uncertainties were calculated in the absolute reference frame (Dennis et al., 2011) following
272 Daëron et al. (2016).

273

274 3. Results

275 3.1 Aragonite-Calcite Phase Transition

276 Given its instability under ambient pressure, aragonite is expected to transform into
277 calcite during our low pressure heating experiments. XRD and Raman spectroscopy
278 measurements confirm this general prediction, although there is significant variation in the
279 reaction progress as a function of time (Figure 2b,e). Similar variations in reaction progress were
280 observed in the XRD powder patterns in the aragonite heating experiments of Staudigel & Swart
281 (2016). This is likely related to the phase transition progressing inhomogeneously through the

282 crystal lattice. Nevertheless, the overall pattern of the time and temperature evolution of the
283 reaction is clear: At 200 and 300°C, we observed negligible production of calcite over the
284 course of our experiments. Significant amounts of newly grown calcite were observed at
285 temperatures of 350°C and above. When the samples were exposed to the ambient air (rather
286 than being heated in a pure CO₂ atmosphere), 80% of the aragonite was converted to calcite in 72
287 hours at 350°C (Experiment SC-C). However, such rapid conversion at this relatively low
288 temperature was atypical; the experiments conducted at 350°C in a CO₂ atmosphere underwent
289 5–25% conversion after 72 hours (Experiment SC-D, SC-E and SC-H). We conclude that when
290 the reaction proceeds in air the phase transformation is accelerated, perhaps due to the presence
291 of water vapor. At 400°C and 450°C, aragonite was mostly converted to calcite within 10 hours.
292 At 500°C, nearly complete conversion to calcite was achieved in 40 minutes (Figure 2e).
293 Previous studies that conducted in-situ XRD and FTIR characterizations of the aragonite to
294 calcite phase transition show a more rapid conversion over a period of ~10 minutes as the
295 temperature is raised to 400–450°C (Antao & Hassan, 2010; Koga et al., 2013). Other
296 experimental studies have found timescales for the phase transition more similar to what we
297 observe, from minutes to hours above 400°C, depending on the sample origin, grain sizes and the
298 experimental method (Davis & Adams, 1965; Madon & Gillet, 1984; Koga et al., 2013;
299 Staudigel & Swart, 2016). Thus, we find a threshold temperature for significant phase transition
300 similar to that observed in previous studies, and rates of conversion that lie at the slower end of
301 the spectrum of values reported in previous work. We suspect that the relatively slow rate of the
302 phase transition measured in our experiments is related to the length scale of the techniques we
303 used to characterize crystal structure for most of our experimental products. XRD (used for only
304 a few of our samples) observes structures that are coherent over hundreds to thousands of unit

305 cells (10^{-8} – 10^{-7} m), whereas Raman spectroscopy (used for most of our samples) observes
306 structural properties at length scales corresponding to the wavelengths of infrared light (10^{-6} m).
307 As a result, phase transitions detected by Raman spectroscopy might be seen to occur later than
308 those detected by XRD (i.e., assuming phase transformation is structurally coherent over longer
309 length scales as time progresses). This suspicion is supported by the observation that our XRD
310 characterization of the phase transition at 400°C indicated that it was completed in two hours,
311 faster than the 450°C experiment measured by Raman spectroscopy.

312

313 *3.2 Clumped Isotope Reordering of Low-Temperature Aragonite*

314 Given the thermodynamic basis for the carbonate clumped isotope thermometer, it is
315 expected that the Δ_{47} value of a carbonate mineral that initially grows at low-temperature and
316 then is subjected to a higher temperature will monotonically decrease in Δ_{47} until it approaches
317 the new, higher temperature equilibrium state of a lower Δ_{47} value (Figure 1a). This behavior
318 was previously observed in calcite, apatite, and dolomite reordering experiments (Passey &
319 Henkes, 2012; Henkes et al., 2014; Stolper & Eiler, 2015; Lloyd et al., 2018; Brenner et al.,
320 2018). The reaction progress of solid-state isotopic reordering we observe in aragonite violates
321 this expectation. Following an initial rapid decrease in Δ_{47} , we observe abrupt increases in Δ_{47} ,
322 with amplitudes in the range of 0.05–0.15 ‰, followed by a more gradual decrease in Δ_{47} values
323 toward the thermodynamic equilibrium values (Figure 2a,d, Figure 4). This complex pattern has
324 amplitudes of initial fall and subsequent rise that are large multiples of our analytical precision,
325 and was observed to be significant and generally homologous in form in all of the experiments in
326 which there was significant contrast between the initial and final equilibrium Δ_{47} values.

327 In our 350°C experiments conducted in both air (SC-C) and CO₂ (SC-D and SC-E), it is
328 clear that there are two separate increases in Δ_{47} in the first 24 hours, separated by an
329 intermediate ‘dip’, and that both of the increases and all three periods of decrease are statistically
330 well resolved (Figure 2a, 4). There is a suggestion that the 450°C experiment conducted in air
331 could also have two separate periods of increasing Δ_{47} , but the first of them is not clearly
332 resolved from the surrounding pattern of decreasing Δ_{47} . Experiments conducted at higher and
333 lower temperatures have only one increase in Δ_{47} during the reordering process.

334 For most series of experiments conducted at one temperature, the first (or only) increase
335 in Δ_{47} observed mid-way through the heating period occurred at the initial stage of the phase
336 transition, i.e., the sample contained less than 20% calcite as determined by XRD or Raman
337 spectroscopy (Figure 4). However, as the proportion of calcite increases (i.e., >20%), the Δ_{47}
338 values decrease again with further heating. Because the timing of the first appearance of calcite
339 and time-evolution in the calcite/aragonite ratio are somewhat irregular in detail, it is not always
340 clear how the rate and direction of change in Δ_{47} relates to the progress of the aragonite to calcite
341 phase transition. However, when we plot the percentage of calcite vs. the Δ_{47} value (a bulk
342 measurement of both aragonite and calcite), it is clear that increases in Δ_{47} occur early in the
343 progress of the aragonite to calcite transition (Figure 4). In summary, the reorganization of ¹³C
344 and ¹⁸O (i.e., changes in Δ_{47} value) that occurs when aragonite is heated can be described as a (at
345 least) three-stage process: initial destruction of ¹³C–¹⁸O bonds (decrease in Δ_{47}), followed by a
346 re-formation of ¹³C–¹⁸O bonds (increase in Δ_{47}), followed by a monotonic decay in ¹³C–¹⁸O
347 bonds until the high temperature equilibrium Δ_{47} value is reached. As noted above, in some
348 experiments, a second cycle of increase and subsequent decrease in Δ_{47} is observed. The stage or
349 stages of heating during which ¹³C–¹⁸O bonds re-form is both a strong departure from

350 thermodynamic equilibrium at the conditions of the experiment, and clearly first occurs during
351 the early stage of aragonite to calcite transition. This pattern is reproducible across a temperature
352 range of more than 100°C. We also note that the Δ_{47} values approach equilibrium at rates that are
353 statistically indistinguishable from the calcite reordering experiments (Passey & Henkes, 2012;
354 Henkes et al., 2014; Stolper & Eiler, 2015) after most of the aragonite has been converted to
355 calcite.

356

357 *3.3 Clumped Isotope Reordering of High-Temperature-Equilibrated Aragonite*

358 The aragonite heated at 600°C at high-pressure for 10 days achieved a clumped isotope
359 composition ($\Delta_{47} = 0.283 \pm 0.016\text{‰}$) that is within error of the expected equilibrium at 600°C
360 ($\Delta_{47_eqm} = 0.273 \pm 0.021\text{‰}$, Bonifacie et al., 2017) (Note that $\delta^{13}\text{C}$ and $\delta^{18}\text{O}$ of this material are
361 similar to other samples of the starting material: 7.43‰ and -7.12‰ , VPDB, respectively;
362 Figure 2f). When this pretreated aragonite was subsequently subjected to a second stage of
363 heating at 350°C in a CO_2 atmosphere, the Δ_{47} increased slightly over the course of 72 hours to
364 the somewhat higher Δ_{47} value expected for equilibrium at 350°C, accompanied by 22%
365 conversion of aragonite to calcite (Figure 2d,e, Figure 4a,d). The amount of phase transition is
366 similar to the untreated low-temperature aragonite going through the same reordering experiment,
367 but we see no evidence for a sharp rise in Δ_{47} in the middle of the second heating period, as
368 occurred when non-pre-treated aragonite was subjected to this same low-pressure heating
369 schedule (Figure 4a,d). A key feature of the high P-T treatment performed on this sample is that
370 it involved a time-at-temperature sufficiently prolonged such that the reaction-diffusion model
371 would predict complete mutual equilibration of all three populations of isotopic species: clumps,
372 pairs and singletons (Figure 1c). This series of experiments demonstrates that the anomalous rise

373 in Δ_{47} associated with conversion of aragonite to calcite does not occur in materials that have
374 already attained a fully equilibrated high-temperature isotopic structure due to a long, high-
375 temperature ‘soak’; that is, this phenomenon requires that the aragonite to calcite transition takes
376 place in a material that has experienced a sharp drop in Δ_{47} within the previous few hours. This
377 finding also indicates that the increase in Δ_{47} does not arise through a kinetic isotope effect
378 associated with the aragonite to calcite transition (i.e., a dependence of the rate of phase
379 transition on the isotopic composition of the carbonate groups).

380

381 *3.4 Clumped Isotope Reordering in a Two-Step Calcite Experiment*

382 After we subjected two samples of calcite to a first heating treatment of 450°C for 5
383 hours, their Δ_{47} values dropped from 0.586‰ to 0.474‰ and 0.426‰, respectively, without
384 significant changes in their bulk $\delta^{13}\text{C}$ or $\delta^{18}\text{O}$ (Table 1, Figure 5). When each of these pre-heated
385 calcites were subjected to a second heat treatment at 500°C, their Δ_{47} values increased by 0.03–
386 0.06‰ in the first 15 minutes of the second heating treatment, before decreasing again
387 afterwards. Interpretation of this experiment must be equivocal as the variations in Δ_{47} that we
388 observe are near the 2 standard error limit of significance. Nevertheless, both experimental series
389 suggest that it is possible to subject calcite to a heating schedule that creates subtle but resolvable
390 increases in Δ_{47} in the absence of a phase transition. The specific heating schedule we selected to
391 create this effect was based on a prediction of the reaction-diffusion model, and this experiment
392 is important to our efforts below to interpret and generalize the more pronounced Δ_{47} increases
393 we observe during the aragonite to calcite transition.

394

395 **4. Discussion**

396 The formation of excess ^{13}C - ^{18}O bonds (producing an increase in Δ_{47}) during high-
397 temperature transformation of aragonite to calcite is a significant, reproducible observation of
398 this study and appears to act opposite to thermodynamic driving forces. Yet it also is not a
399 kinetic isotope effect associated with some elementary step of the phase transformation, as no
400 such isotopic reordering is observed when aragonite is allowed to achieve a fully equilibrated
401 high-temperature isotopic structure prior to transformation to calcite. This phenomenon has not
402 only been reproduced in our experiments, but also resembles the similar (though less regular)
403 findings of previous heating experiments performed on aragonites of different origins (Staudigel
404 & Swart, 2016). Moreover, we see suggestive evidence that the same phenomenon can be made
405 to occur in calcite, absent any phase transformation, provided the calcite is subjected to a specific
406 heating schedule. We find no evidence that any of these effects are accompanied by changes in
407 bulk isotopic content ($\delta^{13}\text{C}$ and $\delta^{18}\text{O}$) that might provide evidence for open system reactions. We
408 suggest that this behavior is an integral feature of solid-state isotopic reordering in carbonate
409 minerals that needs to be incorporated in future reordering models.

410 In the following discussion, we describe how this behavior can be conceptually explained
411 by the reaction-diffusion model of Stolper & Eiler (2015). We also discuss the new insights these
412 findings provide regarding the kinetics of atomic mobility within carbonates and the kinetics of
413 the aragonite to calcite transition. Finally, we use these results to support the presence and
414 significance of pairs in carbonate minerals, and to generalize the reaction-diffusion mechanism
415 across carbonate minerals

416

417 *4.1 The Reaction-Diffusion Model and High-Temperature Formation of Excess ^{13}C - ^{18}O Bonds*

418 Increases in Δ_{47} during a high-temperature heating step are a previously unrecognized
419 prediction of the reaction-diffusion model of Stolper and Eiler (2015). Specifically, we now
420 recognize that this phenomenon is a natural consequence of the fact that disproportionation of
421 clumps to form pairs leads to a brief period of time (typically hours at the temperatures of our
422 experiments) when the pairs have not yet diffused apart to form singletons and have the potential
423 to back-react to re-form clumps (Figure 1b).

424 Stolper and Eiler (2015) proposed the reaction-diffusion model as a way of explaining the
425 kink in the time evolution of decreasing Δ_{47} values; specifically, they suggested that this feature
426 marks the time when the rate of net formation of pairs by breakdown of clumps is nearly
427 balanced by the rate of diffusive separation of pairs to form singletons.

428 We observe several low-pressure time-series where Δ_{47} values rise sharply during the
429 aragonite to calcite transition, with amplitudes of 0.13–0.18‰, or roughly 30–40% of the
430 contrast between the initial Δ_{47} value and the Δ_{47} value the carbonate would have after fully
431 equilibrating at the temperature of the experiment. Interpreted in the context of the reaction-
432 diffusion model, this implies that the reaction of a clump to form a pair largely reverses at the
433 onset of the aragonite to calcite transition (i.e., 50–80% of clumps destroyed during the earliest
434 stage of heating temporarily re-form). For experiments with two separate Δ_{47} increases at 350°C,
435 the second increase is almost a quantitative reversal of the previous drop in Δ_{47} .

436 Perhaps the strongest argument that an intermediate pool of pairs is required to drive Δ_{47}
437 increases at high temperature comes from the lack of a Δ_{47} rise when aragonite is given a long,
438 very high temperature, high pressure ‘soak’ before the aragonite to calcite transition (see section
439 3.3 above). This experiment indicates that the sharp increases in Δ_{47} are only a feature of

440 aragonite that undergoes transformation to calcite immediately (within minutes to hours) after its
441 Δ_{47} has decreased in response to heating.

442 This can be understood as a consequence of the pair mechanism: For all of our
443 experiments involving a single, low-pressure stage of heating, clumps are transformed to pairs
444 early in the experiment, but those pairs have not had enough time to diffusively separate to form
445 singletons, so they are present as a potentially reactive pool of excess pairs when the phase
446 transformation occurs (Figure 1b). In aragonite that has undergone long, high-temperature, high-
447 pressure heating, the pool of pairs has been depleted through diffusion to form singletons,
448 removing that pool of excess pairs (Figure 1c).

449 We hypothesize that the reformation of clumps from an over-abundant pool of pairs is
450 associated with the rearrangement of carbonate ions in the crystal lattice on the unit-cell scale.
451 Several models have been proposed to describe the atomistic mechanism of the aragonite-calcite
452 phase transition. Previous studies agree that this solid-state transition involves displacement of
453 calcium layers relative to carbonate layers, and 30° rotations of carbonate groups (Madon &
454 Gillet, 1984; Antao & Hassan, 2010; Miyake & Kawano, 2010). The rotation of carbonate
455 groups converts the 9-coordinated aragonite structure to the 6-coordinated calcite structure, and
456 clearly involves reorganization of Ca–O bonds (Madon & Gillet, 1984; Miyake & Kawano,
457 2010). However, prior studies did not specify whether this reorganization of the geometries of
458 carbonate ions is accomplished by the breaking and re-forming of C–O bonds or simply involves
459 motions of carbonate ions with respect to one another. Our findings that the aragonite-to-calcite
460 reaction is accompanied by a large change in ^{13}C – ^{18}O ordering suggests that the first possibility
461 is the case.

462 Each O atom in the aragonite lattice has up to eight nearest neighbor O atoms (i.e., those
463 that can be reached in a straight line, omitting those that share the moving atom's own carbonate
464 ion unit, and noting that some sites that are 'adjacent' by this definition are much closer than
465 others; Figure 6a). Thus, if the clump-to-pair transition involved purely random movement of O
466 atoms from one carbonate ion unit to a randomly-selected neighbor, and that the aragonite to
467 calcite transition was accompanied by a second random exchange of an O atom with one of its
468 set of possible 'straight line' nearest neighbors, it should only be possible to recover a small
469 fraction of the original clumped isotope signature (i.e., most ^{18}O atoms that make the first jump
470 away from a clump will not return to their original carbonate ion unit on their second jump; nor
471 are they likely to reach another ^{13}C atom on making a second jump). The fact that most of the Δ_{47}
472 signature that was initially lost is recovered suggests that the transition from clumps to pairs
473 preferentially involves O exchange between only one (or perhaps two) of the possible nearest
474 neighbor pairs, and that the aragonite to calcite transformation is accompanied by an O exchange
475 that takes advantage of that same preferred oxygen site or sites. This might be expected if one of
476 the possible pathways for exchanging an O atom between two carbonate groups has a lower
477 activation energy than any of the other possible exchange mechanisms, and so occurs at a higher
478 rate. In the 9-coordinated aragonite structure, there are five different Ca–O bonds and two non-
479 equivalent oxygen sites, O1 and O2 (Figure 6a; Antao & Hassan, 2010; Ye et al., 2012). The
480 strengths of the Ca–O and C–O bonds for these two oxygen sites are different, which we
481 anticipate could give rise to different activation energies of the various possible oxygen
482 exchange pathways. In particular, the three exchange pathways labeled in Figure 6a involve
483 breaking the weakest bonds in the aragonite structure and, we suggest, could be energetically
484 favorable. Two of these three pathways involve an O1–O2 exchange (pathways 2 and 3 in Figure

485 6a). After exchange through these two pathways, the aragonite-calcite phase transition would
486 keep the singly-substituted carbonate groups in neighboring positions (i.e., remaining as pairs) as
487 shown in Figure 6b. We suggest that quantitative conversion of pairs to clumps can be explained
488 as a two-step mechanism: 1) initial preferential conversion of clumps to pairs along the O1–O2
489 exchange pathway, followed by 2) forced exchange of O1–O2 oxygen atoms during the
490 aragonite to calcite phase transition. This hypothesis is an attractive target for future molecular
491 dynamic models of the kinetics of the CaCO_3 phase transition and solid-state clumped isotope
492 reordering.

493 We also draw attention to the fact that the rise in Δ_{47} that accompanies the aragonite to
494 calcite transition is observed at approximately the time when XRD or Raman evidence for calcite
495 formation is first observed, but well before complete conversion of aragonite to calcite (by which
496 time Δ_{47} has fallen again). It would be rational to argue that this is just the behavior expected if
497 the rise in Δ_{47} reflects a kinetic isotope effect associated with the transition (i.e., a dependence of
498 its rate on the isotopic content of the reacting carbonate ions). However, our experiment
499 performed on aragonite that had been isotopically equilibrated at high pressure shows this is not
500 the case. Isotope exchange between adjacent carbonate ion units happens over atomic length
501 scales (10^{-10} m), whereas XRD and Raman observe structures that are coherent over much longer
502 length scales (10^{-8} – 10^{-6} m). A comparison of the apparent rates of these three measurements of
503 the aragonite to calcite transition at different spatial scales is shown in an Arrhenius plot (Figure
504 7). We see that over our experimental temperature range the rate of initial clump-to-pair
505 conversion in aragonite is faster by an order of magnitude than the rate of XRD determined
506 phase transition, which is in turn an order of magnitude faster than the rate of phase transition
507 estimated by Raman spectroscopy over our experimental temperature range. We suggest that the

508 structural rearrangements involved in the aragonite to calcite transition begin at short length
509 scales and only gradually does the calcite structure become coherent to longer length scales;
510 furthermore, we argue that the clumped isotope composition is sensitive to the earliest, shortest
511 length scale re-arrangements, while XRD and Raman are sensitive to structural re-organization
512 on increasingly longer length scales.

513 The trend in Figure 7 for the rate of clumped isotope reordering in aragonite is not a
514 straight line. This observation suggests that clumped isotope reordering may occur through two
515 or more separate steps that differ in activation energies. This finding may offer insight into why
516 we sometimes see two separate rises in Δ_{47} over the course of the aragonite to calcite transition.
517 The two separate increases in Δ_{47} at 350°C may reflect the fact that we can see two separate steps
518 in a complex bond reordering process because the phase transition is slow, letting us observe
519 isotopic evolution over a gradually spreading conversion of aragonite to calcite; by this
520 interpretation, no clear evidence for two Δ_{47} rises is seen at higher temperatures simply because
521 the phase transition progresses too quickly relative to our sampling interval.

522 In summary, we explain the complex evolution in Δ_{47} values observed when an aragonite
523 that formed at low temperature converts to calcite at high temperature as an interplay between
524 the mechanisms of isotope exchange between clumps, pairs and singletons on one hand and the
525 dynamics of the aragonite-calcite phase transition on the other. The initial reduction in Δ_{47} that
526 occurs when aragonite is first heated but has not yet reacted to form detectable calcite is an
527 exchange between the clumped and unsubstituted carbonate ions to build up pairs in the
528 aragonite lattice. This initial exchange preferentially occurs by an exchange of oxygen between
529 only one (or perhaps two) of the several possible pairs of nearest-neighbor O sites. The
530 subsequent rise in Δ_{47} marks the first detectable stage of conversion of aragonite to calcite, which

531 is associated not only with re-alignment of carbonate ion units but also with the breaking and re-
532 forming of C–O bonds. The first of these bond breaking and re-forming events take advantage of
533 the same low activation energy pathway that is the preferred mechanism of clumped isotope
534 reordering. Thus, the O atom exchange that is forced by the phase transition effectively reverses
535 any immediately preceding conversion of clumps to pairs. The only exception to this pattern is
536 seen when aragonite is allowed to isotopically equilibrate at high temperatures before conversion
537 to calcite, which we take as evidence for slower diffusion-limited separation of pairs to form
538 randomly distributed singletons. We suggest that the observation of two separate periods of
539 increasing Δ_{47} when low-temperature aragonite is converted to calcite at 350°C indicates that this
540 structural re-organization occurs through two or more steps that differ in their rates, but that are
541 only clearly observed when phase transformation is slow yet goes to completion (conditions that
542 are not both met at significantly higher or lower temperatures).

543

544 *4.1.2 Back-reaction of pairs during sharp temperature changes*

545 Our two-step calcite heating experiments were designed to generate pair excesses and
546 drive back-reactions to re-form clumps in the absence of a phase transformation (Figure 1b).
547 During the first stage of the experiments, the samples were heated at 450°C for 5 hours.
548 According to the kinetic parameters derived in Stolper & Eiler (2015), these temperature-time
549 conditions should have allowed the clumps to pairs reaction to go nearly to completion. In
550 contrast, the diffusion-limited separation of pairs to form singletons should not yet have
551 progressed to a significant extent. Thus, a pair excess should have existed at this point. The
552 samples were then exposed to a higher temperature of 500°C, which lowers the equilibrium pair

553 concentration, increasing the driving force for pairs to either separate or back-react to form
554 clumps.

555 The magnitude of the change in Δ_{47} predicted by the reaction-diffusion model for this
556 heating history depends on the excesses above a random distribution for both clumps and pairs
557 prior to any heating (i.e., when the studied sample first crystallized), and the temperature
558 dependence of the equilibrium concentrations for clumps and pairs. These quantities are
559 relatively well known for the clumped isotope species, but are essentially unverified assumptions
560 in the case of pairs. If we adopt the assumed values by Stolper and Eiler (2015) for pairs, and
561 adjust their estimated values for the rate constants, k_f , k_d in Rxn 2 within their stated
562 uncertainties, the model can predict a rise in Δ_{47} during the second stage of this heating
563 experiment (Model-1 in Figure 5) that is similar in timing to the rises we observe, but so muted
564 in amplitude it could not be measured with current analytical methods (whereas we reproducibly
565 observe an effect several times analytical precision). We constructed several alternative model
566 predictions of the consequences of our experimental heating schedule by increasing the
567 temperature sensitivity of the pair excess by a factor of 6 relative to the value assumed by Stolper
568 and Eiler (2015) (Model-4 in Figure 5). A model that closely matches the rate of Δ_{47} decrease in
569 this experiment also requires adjustment of the initial pair concentration, by a few parts in 10^4
570 (see Table 2 and Figure 5). These modifications demonstrate the capacity of the reaction-
571 diffusion model to generate temporary increases in Δ_{47} , but show that quantitatively fitting
572 experimental data requires tuning the parameters that define the abundances and behavior of
573 pairs—parameters that are, at present, poorly constrained. For this reason we consider this set of
574 experiments and the calculations discussed above to provide only suggestive evidence regarding

575 the underlying mechanism that produces the anomalous Δ_{47} rises in calcite during the two-stage
576 heating process.

577 Despite the complexities in and assumptions of the model required to explain the
578 significant Δ_{47} increases, the experimental observations are important for two reasons: 1) they
579 show that anomalous increases in Δ_{47} can occur during heating in the absence of a phase
580 transformation; and 2) they confirm a peculiar prediction of the reaction-diffusion model that
581 arises from the hypothesized existence and properties of pairs. It remains true that we have no
582 direct observations of pairs (nor can we think of a way in which they could be observed with
583 meaningful precision). However, these results suggest that the dynamics of interconversion of
584 clumps, pairs and singletons could be universal to the solid-state isotopic reordering of carbonate
585 minerals (and perhaps other molecular salts).

586 We could not think of a way that the defect-annealing mechanism would be predicted to
587 drive a Δ_{47} increase during heating, against the thermodynamic driving force. Our expectation is
588 that the defect density in a crystal changes the rate of diffusion and thus the time it takes to reach
589 equilibrium, but not the direction of clumped isotope evolution. We observed Δ_{47} reversals
590 against thermodynamic trends in both the aragonite-calcite phase transition and the two-stage
591 calcite heating experiments. While the former may involve creation of new defects as the crystal
592 structure is rearranged, we do not expect significant changes in the number of defects in the same
593 calcite over a short period of time (15 minutes) as the temperature is raised by 50°C. Only the
594 presence of an intermediate pool of pairs can possibly cause the observed clumped isotope
595 reversals.

596 We also note that the observed Δ_{47} increases in calcite are expected only for specific
597 heating pathways, have been observed only for the experiments discussed here, and are of

598 secondary importance to the overall reordering trend. The original pair-diffusion model
599 parameters in Stolper & Eiler (2015) still predict the general trend of our calcite data better than
600 the variety of other parameters that generate Δ_{47} increases (Figure 5), as well as for calcite under
601 a wide range of experimental and geological thermal histories.

602

603 *4.2 Differences Between Aragonite and Calcite in Reordering Kinetics*

604 While the reaction-diffusion reordering mechanism can conceptually explain the
605 complicated clumped isotope reordering pattern in aragonite, it should be noted that the kinetics
606 of clumped isotope reordering in aragonite are distinct from calcite, even in the absence of the
607 aragonite to calcite phase transformation. In our experiments, aragonite clumped isotope
608 reordering is triggered at temperatures much lower than those for calcite. No clumped isotope
609 reordering was observed for calcite up to temperatures of 380°C (Passey & Henkes, 2012;
610 Stolper & Eiler, 2015). In contrast, we see aragonite reordering take place at temperatures as low
611 as 200°C in our experiments, and significant reordering has been observed at even lower
612 temperatures (125°C–175°C) by others (Staudigel & Swart, 2016). Given the complicated
613 reordering pathways and the interplay with the phase transformation, it is challenging to estimate
614 accurate rate constants for clumped isotope reordering in aragonite with the existing data. Using
615 the reaction-diffusion model to fit the data, the initial stage of rapid Δ_{47} decrease by clump-pair
616 conversion in aragonite requires a rate constant (k_f in Rxn 2) that is 1–2 orders of magnitude
617 larger than that in calcite (Figure 7). Large uncertainties remain with these estimates due to the
618 scarcity of data points before the phase transition is triggered to cause a reversal in Δ_{47} . We
619 expect time series experiments of aragonite reordering at high pressure (in its stability field) to
620 provide better estimates of the rate constants. However, it is a robust observation in our

621 experiments that when an aragonite-calcite phase transition is involved, the time it takes for the
622 mineral to reach clumped isotope equilibrium is much shorter than for calcite (Figure 4). For
623 example, it took 500 hours for calcite to reach equilibrium at 430°C (Stolper & Eiler, 2015),
624 while the equilibrium composition was reached in 42 hours in our 450°C experiment as aragonite
625 was converted to calcite (Figure 4). As a result, aragonite's initial clumped isotope composition
626 is predicted to alter at much lower temperatures than that of calcite and dolomite (Stolper & Eiler,
627 2015; Lloyd et al., 2018), making it highly susceptible to moderate heating during early
628 diagenesis. The Δ_{47} increases during heating and phase transition may further complicate the
629 interpretation of clumped isotope compositions of aragonite and aragonite-derived calcite in
630 sedimentary basin settings. Because unit-cell-scale transformations of aragonite to calcite can
631 artificially raise Δ_{47} values, carbonate materials with 'cold' clumped isotope temperatures that
632 appear to be pristine, unmodified aragonite (based on XRD and Raman spectroscopy) may be
633 indistinguishable from aragonite that experienced moderate heating, partially-reordered in the
634 solid-state, and partially transformed to calcite at a scale finer than the above conventional
635 techniques can detect. However, our reordering experiments make it possible to better constrain
636 a quantitative model of clumped isotope reordering in carbonate minerals in general, and
637 potentially will allow a more complete understanding of the temperature history of natural
638 carbonates measured using clumped isotopes.

639 Because aragonite and calcite have the same chemical composition, the difference in
640 reordering kinetics is likely a result of structural differences between the two minerals. We
641 surmise that the rate of isotope exchange in the solid-state is determined by the bonding
642 environment of atoms in the crystal lattice. Aragonite has a more tightly compacted structure
643 compared to calcite, and the shortest pathway between oxygen atoms in neighboring carbonate

644 groups is smaller in aragonite than in calcite. Nevertheless, certain Ca–O and C–O bonds in
645 aragonite are longer and thus weaker in aragonite than in calcite (Antao & Hassan, 2010; Ye et
646 al., 2012). As a result, the pairs in aragonite that originate from disproportionation of a clump
647 may have a lower energetic barrier to form (and to exchange back to the clumped species, in the
648 event that a phase transformation forces an oxygen exchange between neighboring pairs). The
649 bonding environment of oxygen atoms is also less symmetric in aragonite than calcite (Figure 6),
650 which may create multiple pools of pairs at the non-equivalent oxygen sites; we speculate that
651 this diversity of O bonding environments may be related to the fact that we observe two separate
652 Δ_{47} increases when the aragonite to calcite transformation occurs at 350 °C. The factors
653 controlling these elementary kinetic steps could be further investigated by performing reordering
654 experiments of other carbonate minerals of both calcite-type (e.g., siderite, rhodochrosite) and
655 aragonite-type (e.g., strontianite, witherite) structures, as well as developing molecular dynamic
656 models of solid-state isotope exchange.

657

658 5. Conclusions

659 We conducted a series of isotopic reordering experiments in aragonite at different
660 temperatures and observed complicated patterns of decreasing and increasing Δ_{47} values. In
661 general, the reordering pathway can be described as a series of steps in which Δ_{47} initially drops
662 sharply, then rises sharply at the onset of conversion of aragonite to calcite, and finally falls
663 asymptotically toward the high-temperature equilibrium value. We propose that this pattern can
664 be explained with the reaction-diffusion reordering mechanism associated with the aragonite-
665 calcite phase transition. We tested the hypothesis with a reordering experiment on an aragonite
666 sample whose isotopic structure (clumps, pairs and singletons) was equilibrated at high

667 temperature and pressure. The lack of an abrupt rise in Δ_{47} when this sample was subsequently
668 converted to calcite suggests that such Δ_{47} increases require pools of excess pairs. We further
669 tested the presence of pairs in carbonates in general by conducting a two-step calcite heating
670 experiment. After a pretreatment aimed at increasing pair concentrations in calcite, a small but
671 statistically significant rise in Δ_{47} was reproduced during the second stage of the experiment.
672 These experiments suggest a general mechanism of clumped isotope reordering based on the
673 reaction-diffusion model that can be applied to different carbonate minerals.

674 Although the mechanism of clumped isotope reordering in aragonite and calcite may be
675 similar, the kinetics of the reordering reactions is different for the two minerals. Clumped isotope
676 compositions of aragonite are highly susceptible to reordering at moderate heating, and the
677 reordering kinetics is much faster than in calcite and dolomite. This must be taken into account
678 when applying the clumped isotope thermometer to natural aragonite that has gone through early
679 diagenesis. The lower activation energy of clumped isotope reordering in aragonite as compared
680 to calcite may be related to the bonding environment of the oxygen atoms in the crystal lattice
681 associated with its structure. Factors determining the kinetics of isotope exchange in carbonate
682 minerals could be further investigated by reordering experiments of other carbonate minerals, as
683 well as molecular dynamic models of the mobility of different isotopes through crystal structures.

684

685 **Acknowledgments**

686 We thank George Rossman for help with Raman spectroscopy and providing calcite
687 samples. The XRD measurements were performed in Nathan Lewis's lab at Caltech. We thank
688 Alex Lipp for help with the calcite reordering experiments. S.C. would like to acknowledge
689 financial support from China Scholarship Council for Ph.D. study at Caltech. This work was
690 supported by NSF EAR Award #1322058 to J.M.E.

691

ACCEPTED MANUSCRIPT

Table 1 Data from Aragonite and Calcite Clumped Isotope Reordering Experiments

Sample	Temp (°C)	Heat Time (hrs)	$\delta^{13}\text{C}$ (‰,VPDB) ^e	$\delta^{18}\text{O}$ (‰,VPDB) ^e	Calcite% ^f	Δ_{47} (‰,ARF) ^g
SC-A2 ^a	500	0.71	7.055±0.005	-7.665±0.014	97	0.429±0.015
SC-A3	500	0.33	7.548±0.002	-7.022±0.017	32	0.496±0.016
SC-A4	500	0.17	7.308±0.003	-7.518±0.010	12	0.584±0.020
SC-A5	500	0.50	7.668±0.004	-7.050±0.016	85	0.441±0.019
SC-A6	500	0.20	7.014±0.004	-7.283±0.010	17	0.539±0.010
SC-A7	500	1.05	6.996±0.004	-7.674±0.007	98	0.407±0.018
SC-A8	500	0.08	7.016±0.005	-7.583±0.008	8	0.502±0.017
SC-B1	450	1	7.250±0.003	-7.568±0.004	13	0.564±0.015
SC-B2	450	19	7.706±0.002	-7.193±0.009	70	0.473±0.017
SC-B4	450	8.5	7.564±0.003	-7.285±0.009	75	0.499±0.021
SC-B5	450	2	7.316±0.002	-7.527±0.009	24	0.528±0.020
SC-B6	450	3.1	8.110±0.002	-6.917±0.006	7	0.551±0.014
SC-B7	450	6.5	7.241±0.004	-7.634±0.008	92	0.340±0.015
SC-B9	450	13.5	7.572±0.004	-7.448±0.009	91	0.485±0.011
SC-B10	450	42	7.075±0.005	-7.771±0.004	100	0.317±0.017
SC-B11	450	4	7.531±0.003	-7.952±0.008	13	0.504±0.015
SC-B12	450	0.5	7.919±0.003	-7.145±0.006	11	0.655±0.015
SC-B13	450	5	7.440±0.003	-7.865±0.010	64	0.385±0.021
SC-B14	450	62	7.364±0.003	-7.722±0.007	100	0.334±0.023
SC-B15	450	5.5	7.269±0.003	-7.527±0.013	85	0.366±0.022
SC-C2 ^b	350	5	7.585±0.002	-7.370±0.010	14	0.669±0.023
SC-C3	350	13	7.494±0.003	-7.655±0.006	16	0.459±0.013
SC-C4	350	1.02	7.268±0.003	-7.453±0.006	6	0.638±0.013
SC-C5	350	3	6.985±0.003	-7.727±0.004	4	0.490±0.018
SC-C6	350	18.5	7.728±0.005	-7.341±0.017	13	0.537±0.018
SC-C7	350	37	7.696±0.003	-7.268±0.006	17	0.489±0.016
SC-C8	350	45	7.153±0.002	-7.616±0.010	44	0.469±0.017
SC-C9	350	24	7.389±0.002	-6.976±0.010	8	0.566±0.014
SC-C10	350	72	7.150±0.003	-7.696±0.014	54	0.418±0.022
SC-C11	350	9.5	7.105±0.003	-7.397±0.011	11	0.457±0.019
SC-C12	350	100	7.707±0.004	-7.220±0.016	79	0.432±0.019
SC-D1 ^b	350	9	7.142±0.008	-7.464±0.012	6	0.559±0.019
SC-D2	350	1	6.880±0.007	-7.681±0.011	3	0.563±0.024
SC-D3	350	3	7.436±0.010	-7.323±0.014	4	0.696±0.026
SC-D4b	350	18	7.697±0.006	-6.942±0.007	5	0.691±0.020
SC-D5	350	0.5	7.400±0.008	-7.449±0.011	3	0.677±0.030
SC-D6	350	48	7.613±0.004	-6.845±0.008	11	0.602±0.016
SC-D7	350	72	7.064±0.008	-7.202±0.013	26	0.517±0.025
SC-D8	350	6	7.306±0.007	-7.489±0.011	4	0.660±0.028
SC-D8b	350	6	7.483±0.006	-7.257±0.008	4	0.643±0.023
SC-D9	350	24	7.632±0.007	-7.112±0.011	8	0.681±0.021

SC-D10	350	12	7.446±0.004	-7.260±0.007	4	0.596±0.022
SC-E1	350	6	7.549±0.004	-7.123±0.005	3	0.628±0.018
SC-E2	350	9	7.691±0.010	-7.271±0.004	2	0.665±0.015
SC-E3	350	1	7.604±0.002	-7.290±0.004	2	0.698±0.012
SC-E4	350	3	7.320±0.002	-7.289±0.005	2	0.718±0.014
SC-E5	350	18	7.375±0.002	-7.307±0.006	5	0.711±0.017
SC-E6	350	0.5	7.364±0.003	-7.509±0.006	1	0.688±0.012
SC-E7	350	48	7.493±0.005	-7.106±0.004	4	0.618±0.019
SC-E8	350	72	7.246±0.002	-7.333±0.003	5	0.593±0.019
SC-E9	350	24	7.610±0.004	-7.332±0.007	5	0.647±0.013
SC-E10	350	12	7.588±0.004	-7.213±0.003	4	0.680±0.013
SC-H0 ^c	350	0	7.428±0.046	-7.122±0.049	0	0.283±0.016
SC-H1b	350	9	7.361±0.004	-7.196±0.005	6	0.317±0.015
SC-H2b	350	72	7.445±0.004	-7.201±0.009	22	0.316±0.022
SC-H3	350	48	7.639±0.004	-7.029±0.008	9	0.287±0.019
SC-H4	350	1	7.477±0.006	-7.062±0.009	3	0.307±0.020
SC-H5	350	18	7.459±0.005	-7.077±0.008	5	0.279±0.019
SC-H6	350	0.5	7.495±0.005	-6.981±0.008	3	0.294±0.020
SC-H7	350	12	7.388±0.008	-7.153±0.012	5	0.322±0.020
SC-H8	350	3	7.551±0.005	-7.077±0.009	6	0.280±0.019
SC-H9	350	6	7.499±0.005	-7.023±0.008	5	0.281±0.019
SC-H10	350	24	7.440±0.006	-7.006±0.008	13	0.313±0.010
AP-1	200	1	7.707±0.004	-7.428±0.012		0.656±0.027
AP-7	200	18	7.461±0.005	-6.834±0.010		0.649±0.027
AP-15	200	29	7.410±0.004	-7.642±0.008	0	0.661±0.039
AP-C3	200	90	7.374±0.002	-8.002±0.005		0.709±0.027
AP-C1	200	144	6.859±0.003	-8.166±0.004		0.723±0.024
AP-4	300	1	7.233±0.006	-7.928±0.011	0	0.673±0.033
AP-L	300	2	7.327±0.004	-7.700±0.010		0.635±0.031
AP-2	300	13	7.392±0.005	-7.240±0.010	0	0.619±0.041
AP-10	300	41	7.813±0.004	-7.167±0.010		0.720±0.031
AP-D6	300	216	7.001±0.003	-8.037±0.006		0.693±0.028
AP-G	400	1	7.096±0.004	-7.568±0.009	0	0.473±0.009
AP-B4	400	2	6.135±0.005	-7.055±0.010	99	0.503±0.033
AP-E	400	17	7.386±0.004	-7.599±0.006		0.608±0.030
AP-B2	400	24.6	7.292±0.005	-7.793±0.011	1	0.586±0.032
AP-B11	400	48	7.724±0.007	-7.547±0.015	94	0.549±0.029
N21-1a1 ^d	500	0	-1.381±0.028	-16.788±0.080	100	0.474±0.015
N21-1a2	500	0	-1.168±0.068	-16.894±0.030	100	0.426±0.017
N21-1b1	500	0.25	-1.658±0.026	-17.205±0.101	100	0.503±0.018
N21-1b2	500	0.25	-2.296±0.025	-16.641±0.030	100	0.498±0.008
N21-1c1	500	0.5	-1.592±0.048	-17.049±0.134	100	0.424±0.014
N21-1c2	500	0.5	-1.802±0.008	-16.705±0.030	100	0.468±0.007
N21-1d1	500	0.75	-1.879±0.025	-16.936±0.081	100	0.443±0.019

N21-1d2	500	0.75	-1.391±0.036	-17.176±0.030	100	0.439±0.001
N21-1e1	500	3	-1.549±0.026	-16.860±0.124	100	0.361±0.012
N21-1e2	500	3	-2.394±0.020	-16.803±0.030	100	0.406±0.011

- 693 a. Shaded rows represent heating experiments in ambient atmosphere without CO₂ in the headspace.
694 b. Both SC-C and SC-D experiments were conducted at 350°C, and are labeled C-350°C and D-350°C in
695 the figures.
696 c. The SC-H series are reordering experiments with the clumped isotope randomized aragonite, H0
697 represents the composition after the 10-day high-pressure equilibration at 600°C (average of 2 aliquots).
698 The SC-H series and SC-D series were done at the same time under the same conditions.
699 d. The N21-1 series are data from the two-step calcite reordering experiment. The experiment was
700 replicated on two sets of samples. Samples N21-1a1 and N21-1a2 represent the composition after the first
701 step of heating at 450°C for 5 hours.
702 e. Reported as internal standard errors (1σ).
703 f. Mass fraction of calcite was determined with XRD for AP samples, and with Raman
704 spectroscopy for SC samples
705 g. The Δ₄₇ errors are total standard errors (1 SE) calculated following Daëron et al. (2016).
706
707
708

Table 2 A Summary of Two-Stage Calcite Reordering Models in Figure 4

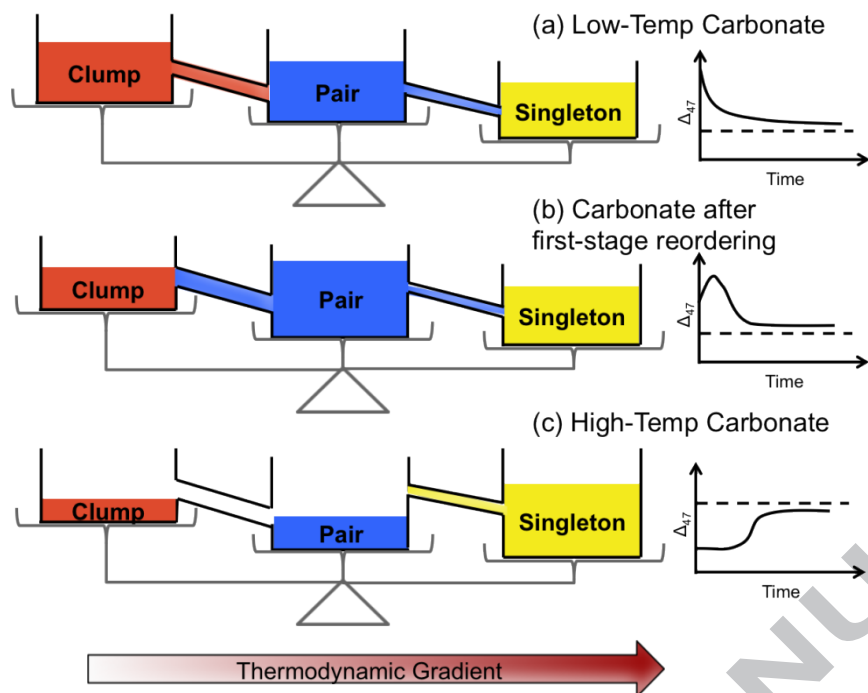
Model	Tuned Variable ^a	Variable Value Relative to Original Model ^b	Timing of 2 nd -Stage Δ ₄₇ Increase (min)	Magnitude of Δ ₄₇ Increase (%)
0	None	Original	N/A	None
1	(k _f , k _d)	(2, 0.5)	5	0.001
2	A	1.6	3	0.0003
3	(A, d _i)	(1.6, 0.99985)	6	0.0005
4	(A, d _i , k _f , k _d)	(6, 0.99918, 2, 2)	13	0.03

- 709 a. For the tuned variables, k_f and k_d represent the rate constants for isotope exchange in Rxn 2.
710 'A' represents the temperature sensitivity of the equilibrium pair concentration presented in the
711 reaction-diffusion model of Stolper & Eiler (2015), following the equation:

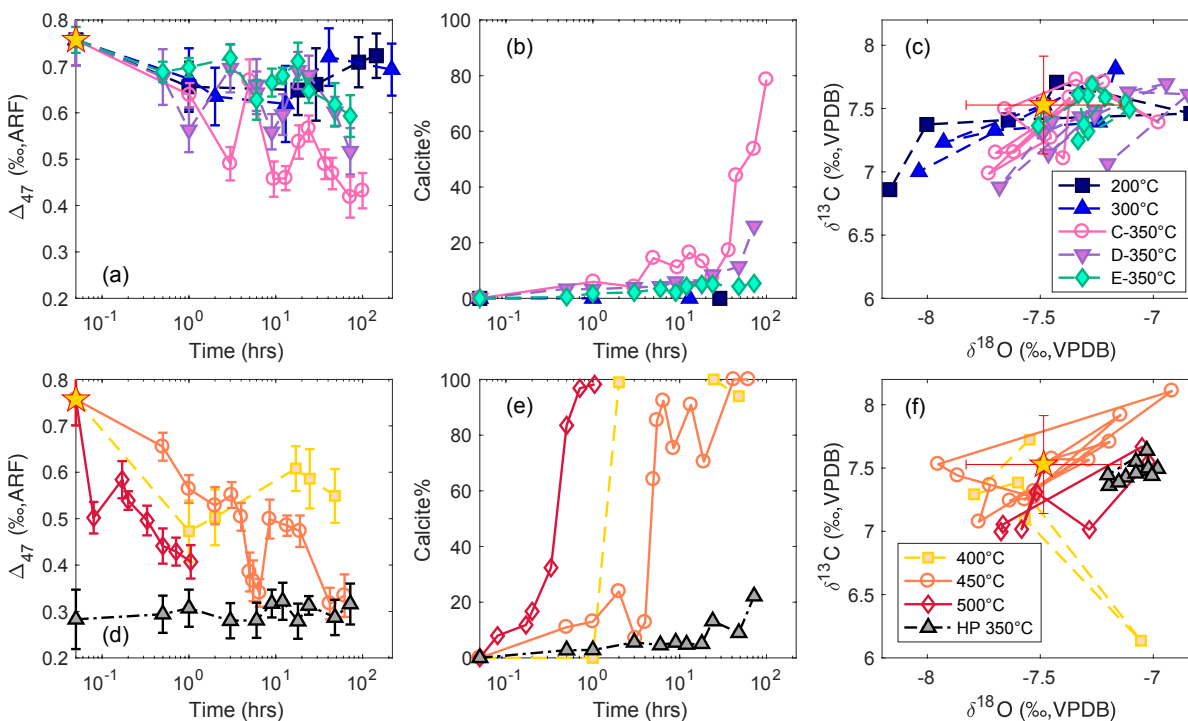
$$\ln [pair]_{eqm}(T) / [pair]_{random} = A/T.$$

- 713 The variable 'd_i' represents an additional variable introduced to account for potential differences
714 in initial pair concentration of different calcite minerals, and to better fit the data of the first-
715 stage of reordering in our experiment. In Model-3 and Model-4, [pair]_{initial} = d_i[pair]_{eqm}.

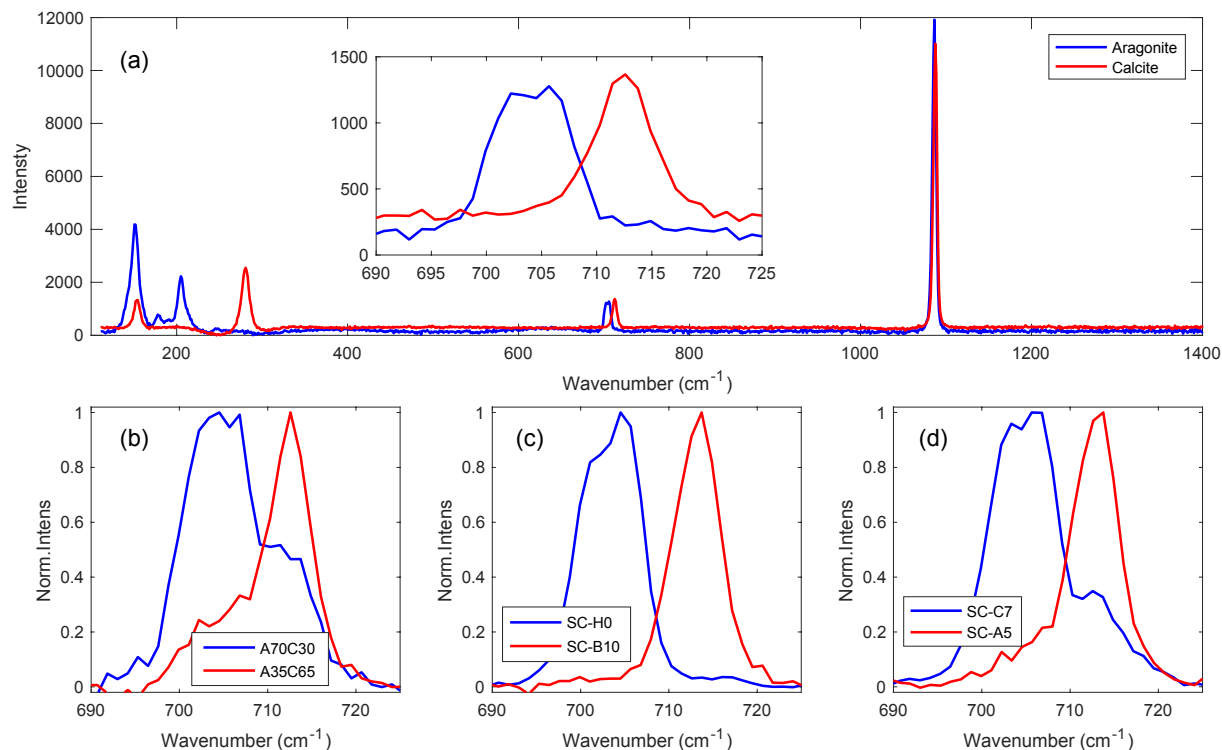
- 716 b. Values represent a multiplication factor applied to the original reaction-diffusion model
717 parameters.



718
 719 **Figure 1** A fluid flow analogy to the reaction-diffusion model as applied to different reordering
 720 experiments in this study. In the model, there are three pools of isotopically substituted carbonate
 721 groups in carbonate minerals: clumps, pairs and singletons, shown as fluids of different colors.
 722 The directions of the reactions (fluid flow) depend on two things: the fluid levels and the vertical
 723 positions of the tanks. The fluid level corresponds to actual concentrations of these carbonate
 724 groups, and the relative base height of the tanks corresponds to the thermodynamic trend. The
 725 plots on the right column show expected clumped isotope reordering patterns in a controlled
 726 heating experiment based on the abundance of clumps, pairs and singletons in each case. **(a)** This
 727 scenario represents a low-temperature carbonate, like the untreated starting material in the
 728 experiment. When exposed to high temperatures, the thermodynamic gradient drives the reaction
 729 from clumps to pairs and pairs diffuse away to form singletons, with a decrease in Δ_{47} over time.
 730 **(b)** This scenario represents a mineral that has been heated for a relatively short amount of time.
 731 In this case, pairs build up in the mineral at the expense of clumps. The pairs may diffuse to fill
 732 the singleton tank, but this process has a higher kinetic limit (thinner tube between blue and
 733 yellow), so that the build-up of pairs exceeds the formation of singletons. The pretreated calcite
 734 in our experiment may represent this scenario, with pairs building up in excess of equilibrium,
 735 and could remake clumps when a higher temperature is imposed. A similar scenario may explain
 736 Δ_{47} increases in aragonite as phase transition is triggered. The multi-stage reordering in aragonite
 737 is a likely combination of (a) and (b). An analogy for pair-excess created by phase transition may
 738 be a shrink in the size of the tank for pairs due to a rearrangement of carbonate ions in the lattices.
 739 The difference between the two minerals may also be related to different reaction rates (size of
 740 connection tubes), or different responses of the equilibrium pair concentration (vertical position
 741 of tanks) to the thermodynamic gradient. **(c)** This scenario represents the aragonite equilibrated
 742 at high temperatures. The equilibration process destroys most clumps and separates pairs into
 743 singletons, and the reordering reaction only goes in the reverse direction afterwards at a lower
 744 temperature. Clump formation can only happen when excess pairs build up, and a buffering time
 745 is expected for an increase in Δ_{47} to be observed.



746
 747 **Figure 2** Isotope and mineralogy data of the aragonite reordering experiments. Panels (a)-(c)
 748 show results of the ambient pressure experiments between 200°C and 350°C, while panels (d)-(f)
 749 show results of the ambient pressure experiments between 400°C and 500°C together with the
 750 350°C reordering experiment on the high pressure high temperature (600°C) equilibrated
 751 aragonite. (a, d) Clumped isotope composition evolution with time (2σ error bars). The star
 752 represents the starting composition of the aragonite. At each temperature, increases in Δ_{47} values
 753 of 0.05–0.15‰ during the heating process are observed in the ambient pressure experiments. The
 754 black triangles represent the reordering experiment starting with clumped isotope randomized
 755 aragonite. Three heating experiments (C-350°C, 450°C, 500°C) were conducted in air (open
 756 symbols) while others were conducted in CO_2 atmosphere (filled symbols). (b, e) Percentage of
 757 calcite in the samples determined by XRD (200°C, 300°C, 400°C) or Raman spectroscopy (other
 758 experiments). There is scatter in the proportions of calcite from the XRD and Raman
 759 measurements, but in general there is an increase in calcite% with time in all experiments above
 760 300°C. (c, f) $\delta^{13}\text{C}$ and $\delta^{18}\text{O}$ values of the reordering experiments. The stars show the initial
 761 composition of the aragonite with 2σ standard deviations. The data points are connected in the
 762 order of heating time. Most data points scatter within the 2σ range of the initial composition of
 763 the aragonite ($\delta^{13}\text{C} = 7.53 \pm 0.17\text{‰}$ and $\delta^{18}\text{O} = -7.49 \pm 0.19\text{‰}$), and no systematic trend is
 764 observed, suggesting closed system behavior during the reordering experiments.



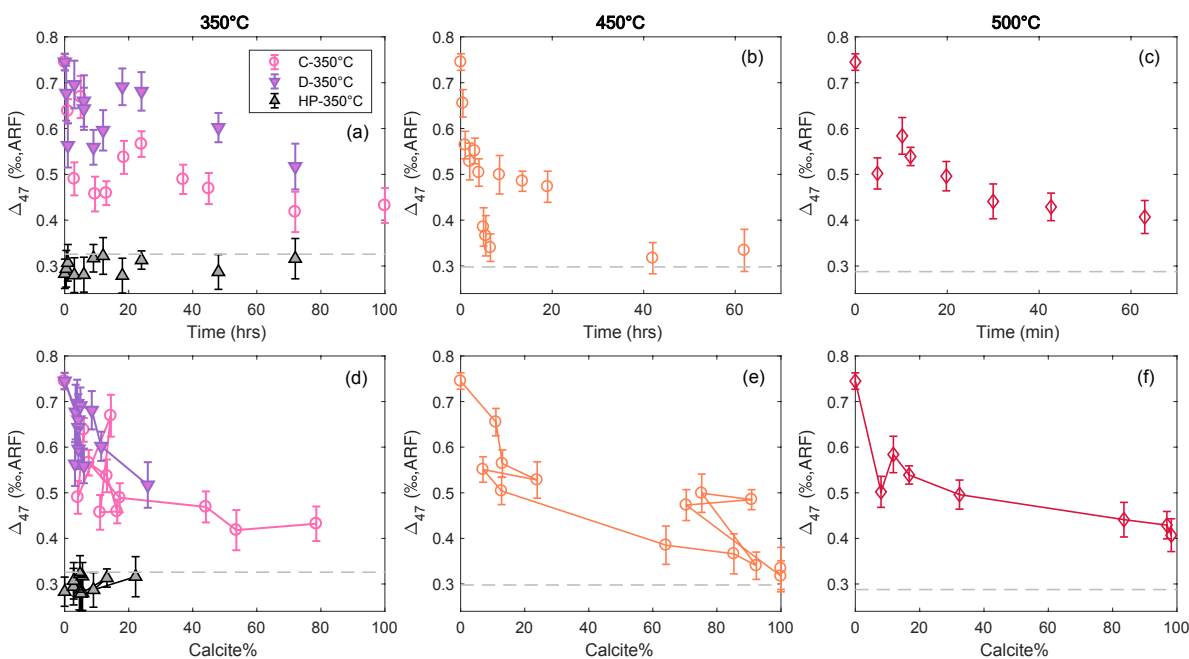
766

767 **Figure 3** Examples of Raman spectra used to determine fractions of aragonite and calcite in the
 768 samples. (a) Full spectra of pure aragonite (blue) and calcite (red), with the inset zooming in to
 769 the wavenumber range of carbonate ion planar bending mode, used to determine relative
 770 abundance of aragonite (704 cm^{-1}) and calcite (713 cm^{-1}) in the samples. (b) Spectra of powder
 771 mixtures of aragonite and calcite used as calibration standards. Examples shown here are a 70:30
 772 aragonite:calcite mixture (blue) and a 35:65 aragonite:calcite mixture. (c) Spectra of samples
 773 from two experiments. SC-H0 is an aragonite sample whose clumped isotope composition was
 774 equilibrated at high temperature (600°C) and high pressure (1.7 GPa). These P-T conditions
 775 preserved its aragonite structure. SC-B10 is a sample that has been completely converted to
 776 calcite after heating at 450°C for 42 hours. (d) Spectra of samples from two other experiments.
 777 SC-C7 was heated at 350°C for 37 hours, and was determined to have 17% calcite by peak area.
 778 SC-A5 was heated at 500°C for 30 minutes, and has 85% calcite.

779

780

781



782

783

784

785

786

787

788

789

790

791

792

793

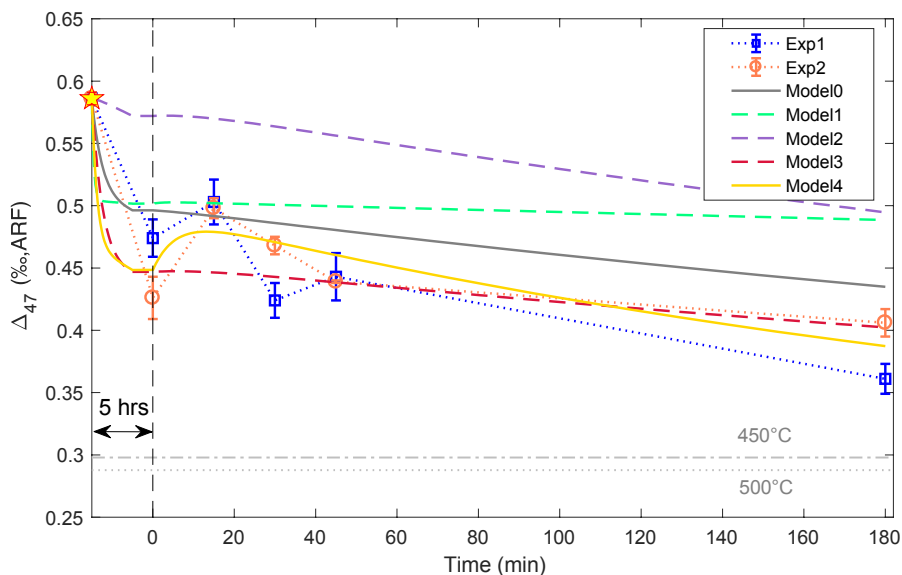
794

795

796

Figure 4 Clumped isotope reordering paths with time (a-c) and percentage of calcite (d-f) in the sample for the experiments at 350°C, 450°C, and 500°C. The lines in panels (d-f) connect points in the order of increasing running time. There are apparent reversals in calcite% with time in panels (d) and (e), which represent noise in the phase transition data at 350°C and 450°C. These reversals are more pronounced for experiments conducted in air (C-350°C and 450°C). Increases in Δ_{47} of 0.05–0.15‰ can be observed during each of the experiments, generally in the range of 0–20% phase transition. The experiments at 350°C (C with ambient atmosphere, D and HP with CO₂ atmosphere) have slightly different magnitudes of Δ_{47} reordering with time, but the reordering paths are similar when calcite% is used as the x-axis, suggesting the reordering kinetics is related to the rate of phase transition. The gray triangles are reordering experiments at 350°C with the clumped isotope randomized aragonite. The dashed lines mark the equilibrium Δ_{47} values at 350°C, 450°C and 500°C respectively (Bonifacie et al., 2017). Note that the x-axis for the 500°C experiment in panel (c) is in minutes.

797



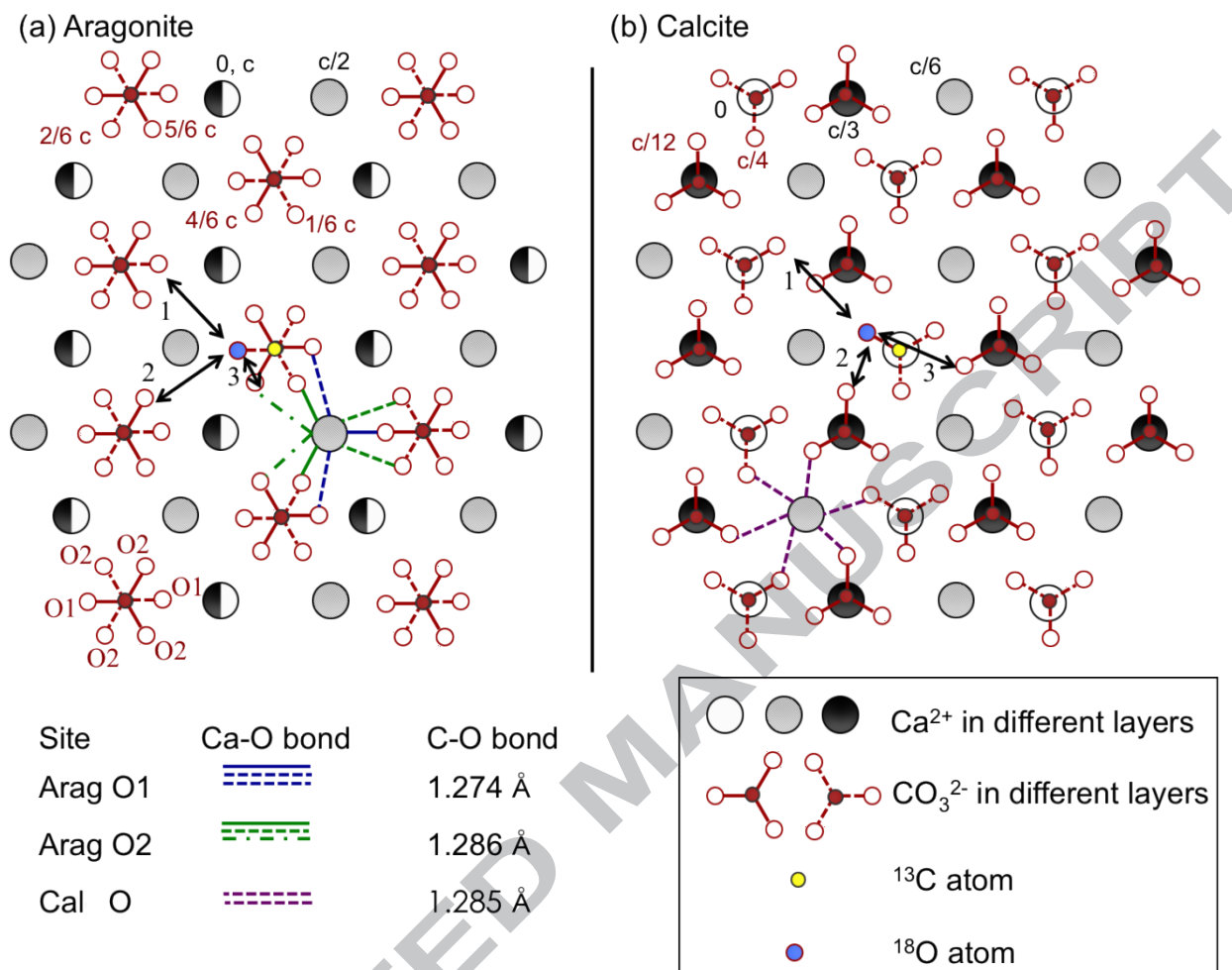
798

799 **Figure 5** Clumped isotope reordering in the two-step calcite heating experiment compared to
 800 model calculations from the reaction-diffusion model (Stolper & Eiler, 2015). The squares and
 801 circles (connected by dotted lines) are replicate reordering experiments at 500°C (second step),
 802 to the calcite that was pretreated by heating at 450°C for 5 hours (first step). The star marks the
 803 initial composition of the calcite. The vertical line separates the two steps. To the left of the line
 804 is the Δ_{47} change with the pretreatment at 450°C for 5 hours (time is not to scale with the second
 805 step on the x-axis). The Δ_{47} value at time zero represents the composition after the pretreatment.
 806 The dash-dot and dotted horizontal lines mark the thermodynamic equilibrium values at 450°C
 807 and 500°C (Bonifacie et al., 2017). In both 500°C reordering experiments, the Δ_{47} values
 808 increased by 0.03–0.06‰ after 15 minutes of the second stage, before decreasing toward
 809 equilibrium. The solid and dashed curves are model outputs from the reaction-diffusion model
 810 with different parameter combinations. The model parameters for each case are listed in Table 2.
 811 Significant changes to the original model parameters in Stolper & Eiler (2015) are required to
 812 generate a curve that fits the data with a well-resolved Δ_{47} increase at the beginning of the second
 813 stage (solid gold curve).

814

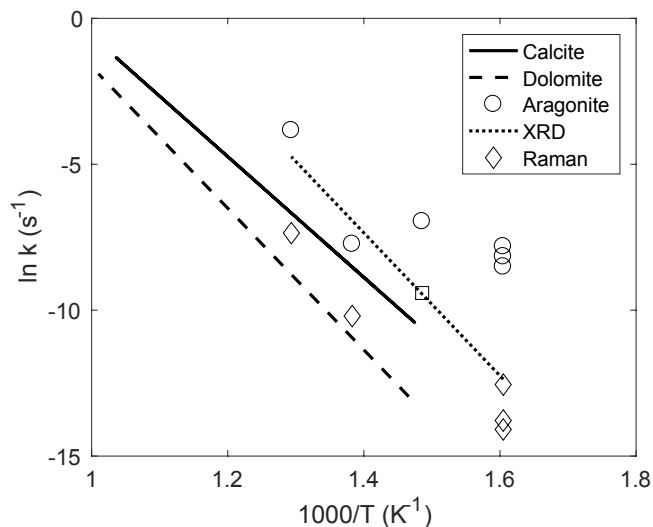
815

816



817
 818 **Figure 6** Comparison of aragonite and calcite mineral structures. The structures are presented as
 819 projections along the c-axis of the minerals, modified from Madon & Gillet (1984). The
 820 positions of Ca²⁺ and CO₃²⁻ along the c-axis are marked in the top two rows of the projected
 821 structures. The half filled Ca²⁺ ions in (a) represent overlapping layers at position 0 and c along
 822 the c-axis. The ¹⁸O and ¹³C atoms are marked by a different color, and are bonded here as a
 823 clumped isotopologue. The blue, green and purple lines show the Ca–O bond in the minerals.
 824 While all Ca–O bonds in calcite are equivalent, there are five different Ca–O bonds in the 9-
 825 coordinated aragonite structure, which gives rise to two non-equivalent oxygen sites O1 and O2.
 826 The length of the C–O bonds associated with O1 and O2 sites are listed in the lower left portion
 827 of the figure. O1 is more loosely bonded to Ca²⁺ with a slightly stronger C–O bond. In panel (a),
 828 the double headed arrows show 3 different pathways for possible preferential oxygen exchange
 829 pathways that involve breaking the fewest and weakest bonds. Pathway 1 is an O1-O1 exchange,
 830 while pathways 2 and 3 are O1-O2 exchange. In panel (b), the arrows show the same exchange
 831 pathways as in (a) after the mineral structure is rearranged. The O1-O2 exchange pathways in (a)
 832 have pairs remaining in neighboring positions after the phase transition in (b), and may cause the
 833 Δ_{47} increases observed during phase transition by a forced back-exchange.

834



835
 836 **Figure 7** Arrhenius plot of clumped isotope reordering and CaCO_3 phase transition kinetics. The
 837 solid and dashed line represents the rate constants of clump to pair conversion (k_f in Rxn 2)
 838 calculated from calcite (Stolper & Eiler, 2015) and dolomite (Lloyd et al., 2018) reordering
 839 experiments. The circles represent rate constants (k_f) for aragonite estimated by fitting the first
 840 stage of Δ_{47} decrease (before the first Δ_{47} increase as phase transition is triggered) in the
 841 experimental data with the reaction-diffusion framework. Clumped isotope reordering in
 842 aragonite is faster than calcite and dolomite. The dotted line represents rates of aragonite-calcite
 843 phase transition at 1 atm calculated from XRD measurements by Davis & Adams (1965). The
 844 estimated rate of phase transition measured by XRD in our 400°C experiment (square) is
 845 consistent with the literature values. The diamonds represent rates of phase transition measured
 846 by Raman spectroscopy in our experiments. Detection of the phase transition by Raman
 847 spectroscopy postdates XRD measurements, and the rate of the aragonite to calcite transition as
 848 determined using either method is slower than the rate of the clumped isotope reordering
 849 reactions in aragonite. The rate constants for phase transition are estimated by $k = 1/\tau$, where τ is
 850 the e-folding time (63.2% reaction progress) of the transition. An exponential curve was fit to the
 851 noisy reaction progress data to estimate the rate of phase transition.
 852

853 **References**

- 854 Antao, S. M., & Hassan, I. (2010). Temperature Dependence of the Structural Parameters in the
855 Transformation of Aragonite to Calcite, as Determined from in Situ Synchrotron Powder X-
856 Ray-Diffraction Data. *The Canadian Mineralogist*, 48(5), 1225–1236.
857 <https://doi.org/10.3749/canmin.48.5.1225>
- 858 Bischoff, J. L. (1965). Temperature controls on aragonite-calcite transformation in aqueous
859 solution. *American Mineralogist*, 54, 149–155.
- 860 Bonifacie, M., Calmels, D., Eiler, J. M., Horita, J., Chaduteau, C., Vasconcelos, C., Agrinier, P.,
861 Katz, A., Passey, B.H., Ferry, J.M., & Bourrand, J.-J. (2017). Calibration of the dolomite
862 clumped isotope thermometer from 25 to 350 °C, and implications for a universal
863 calibration for all (Ca, Mg, Fe)CO₃ carbonates. *Geochimica et Cosmochimica Acta*, 200,
864 255–279. <https://doi.org/10.1016/j.gca.2016.11.028>
- 865 Brand, W. A., Assonov, S. S., & Coplen, T. B. (2010). Correction for the 17O interference in
866 $\delta(13C)$ measurements when analyzing CO₂ with stable isotope mass spectrometry (IUPAC
867 Technical Report). *Pure and Applied Chemistry*, 82, 1719–1733.
868 <https://doi.org/10.1351/pac-rep-09-01-05>
- 869 Brenner, D. C., Passey, B. H., & Stolper, D. A. (2018). Influence of water on clumped-isotope
870 bond reordering kinetics in calcite. *Geochimica et Cosmochimica Acta*, 224, 42–63.
871 <https://doi.org/10.1016/j.gca.2017.12.026>
- 872 Budd, D. A. (1988). Aragonite-to-calcite transformation during fresh-water diagenesis of
873 carbonates: Insights from pore-water chemistry. *GSA Bulletin*, 100(8), 1260–1270.
874 [https://doi.org/10.1130/0016-7606\(1988\)100<1260:ATCTDF>2.3.CO;2](https://doi.org/10.1130/0016-7606(1988)100<1260:ATCTDF>2.3.CO;2)
- 875 Carlson, W. D. (1980). The calcite-aragonite equilibrium: effects of Sr substitution and anion
876 orientational disorder. *American Mineralogist*, 65, 1252–1262.
- 877 Cummins, R. C., Finnegan, S., Fike, D. A., Eiler, J. M., & Fischer, W. W. (2014). Carbonate
878 clumped isotope constraints on Silurian ocean temperature and seawater $\delta^{18}O$. *Geochimica*
879 *et Cosmochimica Acta*, 140, 241–258. <https://doi.org/10.1016/j.gca.2014.05.024>
- 880 Daëron, M., Blamart, D., Peral, M., & Affek, H. P. (2016). Absolute isotopic abundance ratios
881 and the accuracy of $\Delta 47$ measurements. *Chemical Geology*, 442, 83–96.
882 <https://doi.org/10.1016/j.chemgeo.2016.08.014>
- 883 Davis B.L., & Adams, L.H. (2012). Kinetics of the calcite \rightleftharpoons aragonite transformation. *Journal of*
884 *Geophysical Research*, 70(2), 433–441. <https://doi.org/10.1029/JZ070i002p00433>
- 885 Dennis, Kate J., Affek, H. P., Passey, B. H., Schrag, D. P., & Eiler, J. M. (2011). Defining an
886 absolute reference frame for ‘clumped’ isotope studies of CO₂. *Geochimica et*
887 *Cosmochimica Acta*, 75(22), 7117–7131. <https://doi.org/10.1016/j.gca.2011.09.025>
- 888 Dennis, Kate J., & Schrag, D. P. (2010). Clumped isotope thermometry of carbonatites as an
889 indicator of diagenetic alteration. *Geochimica et Cosmochimica Acta*, 74(14), 4110–4122.
890 <https://doi.org/10.1016/j.gca.2010.04.005>
- 891 Dennis, K.J., Cochran, J. K., Landman, N. H., & Schrag, D. P. (2013). The climate of the Late
892 Cretaceous: New insights from the application of the carbonate clumped isotope
893 thermometer to Western Interior Seaway macrofossil. *Earth and Planetary Science Letters*,
894 362, 51–65. <https://doi.org/10.1016/j.epsl.2012.11.036>
- 895 Dickinson, S. R., & McGrath, K. M. (2001). Quantitative determination of binary and tertiary
896 calcium carbonate mixtures using powder X-ray diffraction. *The Analyst*, 126(7), 1118–
897 1121. <https://doi.org/10.1039/b103004n>

- 898 Eiler, J. M. (2007). “Clumped-isotope” geochemistry—The study of naturally-occurring,
899 multiply-substituted isotopologues. *Earth and Planetary Science Letters*, 262(3), 309–327.
900 <https://doi.org/10.1016/j.epsl.2007.08.020>
- 901 Eiler, J. M. (2011). Paleoclimate reconstruction using carbonate clumped isotope thermometry.
902 *Quaternary Science Reviews*, 30(25), 3575–3588.
903 <https://doi.org/10.1016/j.quascirev.2011.09.001>
- 904 Ferry, J. M., Passey, B. H., Vasconcelos, C., & Eiler, J. M. (2011). Formation of dolomite at 40–
905 80 °C in the Latemar carbonate buildup, Dolomites, Italy, from clumped isotope
906 thermometry. *Geology*, 39(6), 571–574. <https://doi.org/10.1130/G31845.1>
- 907 Gallagher, T. M., Sheldon, N. D., Mauk, J. L., Petersen, S. V., Gueneli, N., & Brocks, J. J.
908 (2017). Constraining the thermal history of the North American Midcontinent Rift System
909 using carbonate clumped isotopes and organic thermal maturity indices. *Precambrian*
910 *Research*, 294, 53–66. <https://doi.org/10.1016/j.precamres.2017.03.022>
- 911 Ghosh, P., Adkins, J., Affek, H., Balta, B., Guo, W., Schauble, E. A., Schrag, D., & Eiler, J. M.
912 (2006). 13C–18O bonds in carbonate minerals: A new kind of paleothermometer.
913 *Geochimica et Cosmochimica Acta*, 70(6), 1439–1456.
914 <https://doi.org/10.1016/j.gca.2005.11.014>
- 915 Guo, W., Mosenfelder, J. L., Goddard, W. A., & Eiler, J. M. (2009). Isotopic fractionations
916 associated with phosphoric acid digestion of carbonate minerals: Insights from first-
917 principles theoretical modeling and clumped isotope measurements. *Geochimica et*
918 *Cosmochimica Acta*, 73(24), 7203–7225. <https://doi.org/10.1016/j.gca.2009.05.071>
- 919 Henkes, G. A., Passey, B. H., Grossman, E. L., Shenton, B. J., Pérez-Huerta, A., & Yancey, T. E.
920 (2014). Temperature limits for preservation of primary calcite clumped isotope
921 paleotemperatures. *Geochimica et Cosmochimica Acta*, 139, 362–382.
922 <https://doi.org/10.1016/j.gca.2014.04.040>
- 923 Henkes, G. A., Passey, B. H., Grossman, E. L., Shenton, B. J., Yancey, T. E., & Pérez-Huerta, A.
924 (2018). Temperature evolution and the oxygen isotope composition of Phanerozoic oceans
925 from carbonate clumped isotope thermometry. *Earth and Planetary Science Letters*, 490,
926 40–50. <https://doi.org/10.1016/j.epsl.2018.02.001>
- 927 Huntington, K. W., Eiler, J. M., Affek, H. P., Guo, W., Bonifacie, M., Yeung, L. Y., ... Came, R.
928 (2009). Methods and limitations of ‘clumped’ CO₂ isotope (Δ_{47}) analysis by gas-source
929 isotope ratio mass spectrometry. *Journal of Mass Spectrometry*, 44(9), 1318–1329.
930 <https://doi.org/10.1002/jms.1614>
- 931 Huntington, Katharine W., Budd, D. A., Wernicke, B. P., & Eiler, J. M. (2011). Use of Clumped-
932 Isotope Thermometry To Constrain the Crystallization Temperature of Diagenetic Calcite.
933 *Journal of Sedimentary Research*, 81(9–10), 656–669.
- 934 Ingalls, M. (2019). Reconstructing carbonate alteration histories in orogenic sedimentary basins:
935 Xigaze forearc, southern Tibet. *Geochimica et Cosmochimica Acta*.
936 <https://doi.org/10.1016/j.gca.2019.02.005>
- 937 Jamieson, J. C. (1953). Phase Equilibrium in the System Calcite-Aragonite. *The Journal of*
938 *Chemical Physics*, 21(8), 1385–1390. <https://doi.org/10.1063/1.1699228>
- 939 Koga, N., Kasahara, D., & Kimura, T. (2013). Aragonite Crystal Growth and Solid-State
940 Aragonite–Calcite Transformation: A Physico–Geometrical Relationship via Thermal
941 Dehydration of Included Water. *Crystal Growth & Design*, 13(5), 2238–2246.
942 <https://doi.org/10.1021/cg400350w>

- 943 Lacroix, B., & Niemi, N. A. (2019). Investigating the effect of burial histories on the clumped
944 isotope thermometer: An example from the Green River and Washakie Basins, Wyoming.
945 *Geochimica et Cosmochimica Acta*, 247, 40–58. <https://doi.org/10.1016/j.gca.2018.12.016>
- 946 Lloyd, M. K., Eiler, J. M., & Nabelek, P. I. (2017). Clumped isotope thermometry of calcite and
947 dolomite in a contact metamorphic environment. *Geochimica et Cosmochimica Acta*, 197,
948 323–344. <https://doi.org/10.1016/j.gca.2016.10.037>
- 949 Lloyd, M. K., Ryb, U., & Eiler, J. M. (2018). Experimental calibration of clumped isotope
950 reordering in dolomite. *Geochimica et Cosmochimica Acta*, 242, 1–20.
951 <https://doi.org/10.1016/j.gca.2018.08.036>
- 952 Madon, M., & Gillet, P. (1984). A theoretical approach to the kinetics of calcite \rightleftharpoons aragonite
953 transition: application to laboratory experiments. *Earth and Planetary Science Letters*,
954 67(3), 400–414. [https://doi.org/10.1016/0012-821X\(84\)90178-X](https://doi.org/10.1016/0012-821X(84)90178-X)
- 955 Miyake, A., & Kawano, J. (2010). High-temperature molecular dynamics simulation of
956 aragonite. *Journal of Physics: Condensed Matter*, 22(22), 225402.
- 957 Passey, B. H., Levin, N. E., Cerling, T. E., Brown, F. H., & Eiler, J. M. (2010). High-temperature
958 environments of human evolution in East Africa based on bond ordering in paleosol
959 carbonates. *Proceedings of the National Academy of Sciences*, 107(25), 11245–11249.
960 <https://doi.org/10.1073/pnas.1001824107>
- 961 Passey, B. H., & Henkes, G. A. (2012). Carbonate clumped isotope bond reordering and
962 geospeedometry. *Earth and Planetary Science Letters*, 351–352, 223–236.
963 <https://doi.org/10.1016/j.epsl.2012.07.021>
- 964 Rodríguez-Sanz, L., Bernasconi, S. M., Marino, G., Heslop, D., Müller, I. A., Fernandez, A., ...
965 Rohling, E. J. (2017). Penultimate deglacial warming across the Mediterranean Sea revealed
966 by clumped isotopes in foraminifera. *Scientific Reports*, 7(1), 16572.
967 <https://doi.org/10.1038/s41598-017-16528-6>
- 968 Ryb, U., & Eiler, J. M. (2018). Oxygen isotope composition of the Phanerozoic ocean and a
969 possible solution to the dolomite problem. *Proceedings of the National Academy of*
970 *Sciences*, 115(26), 6602–6607. <https://doi.org/10.1073/pnas.1719681115>
- 971 Ryb, U., Lloyd, M. K., Stolper, D. A., & Eiler, J. M. (2017). The clumped-isotope geochemistry
972 of exhumed marbles from Naxos, Greece. *Earth and Planetary Science Letters*, 470, 1–12.
973 <https://doi.org/10.1016/j.epsl.2017.04.026>
- 974 Schauer, A. J., Kelson, J., Saenger, C., & Huntington, K. W. (2016). Choice of ^{17}O correction
975 affects clumped isotope (Δ_{47}) values of CO_2 measured with mass spectrometry: ^{17}O
976 correction affects CO_2 clumped isotopes. *Rapid Communications in Mass Spectrometry*,
977 30(24), 2607–2616. <https://doi.org/10.1002/rcm.7743>
- 978 Shenton, B. J., Grossman, E. L., Passey, B. H., Henkes, G. A., Becker, T. P., Laya, J. C., Perez-
979 Huerta, A., Becker, S.P., & Lawson, M. (2015). Clumped isotope thermometry in deeply
980 buried sedimentary carbonates: The effects of bond reordering and recrystallization. *GSA*
981 *Bulletin*, 127(7–8), 1036–1051. <https://doi.org/10.1130/B31169.1>
- 982 Staudigel, P. T., & Swart, P. K. (2016). Isotopic behavior during the aragonite-calcite transition:
983 Implications for sample preparation and proxy interpretation. *Chemical Geology*, 442, 130–
984 138. <https://doi.org/10.1016/j.chemgeo.2016.09.013>
- 985 Stolper, D. A., & Eiler, J. M. (2015). The kinetics of solid-state isotope-exchange reactions for
986 clumped isotopes: A study of inorganic calcites and apatites from natural and experimental
987 samples. *American Journal of Science*, 315(5), 363–411.

- 988 Thiagarajan, N., Adkins, J., & Eiler, J. (2011). Carbonate clumped isotope thermometry of deep-
989 sea corals and implications for vital effects. *Geochimica et Cosmochimica Acta*, 75(16),
990 4416–4425. <https://doi.org/10.1016/j.gca.2011.05.004>
- 991 Thiagarajan, N., Subhas, A. V., Southon, J. R., Eiler, J. M., & Adkins, J. F. (2014). Abrupt pre-
992 Bølling–Allerød warming and circulation changes in the deep ocean. *Nature*, 511(7507),
993 75–78. <https://doi.org/10.1038/nature13472>
- 994 Tripathi, A. K., Sahany, S., Pittman, D., Eagle, R. A., Neelin, J. D., Mitchell, J. L., & Beaufort, L.
995 (2014). Modern and glacial tropical snowlines controlled by sea surface temperature and
996 atmospheric mixing. *Nature Geoscience*, 7, 205.
- 997 Wang, Z., Schauble, E. A., & Eiler, J. M. (2004). Equilibrium thermodynamics of multiply
998 substituted isotopologues of molecular gases. *Geochimica et Cosmochimica Acta*, 68(23),
999 4779–4797. <https://doi.org/10.1016/j.gca.2004.05.039>
- 1000 Winkelstern, I. Z., & Lohmann, K. C. (2016). Shallow burial alteration of dolomite and limestone
1001 clumped isotope geochemistry. *Geology*, 44(6), 467–470. <https://doi.org/10.1130/G37809.1>
- 1002 Ye, Y., Smyth, J. R., Boni, P. (2012). Crystal structure and thermal expansion of aragonite-group
1003 carbonates by single-crystal X-ray diffraction. *American Mineralogist*, 97, 707–712.
1004 <http://dx.doi.org/10.2138/am.2012.3923>
- 1005 Zhang, H., Cai, Y., Tan, L., Qin, S., & An, Z. (2014). Stable isotope composition alteration
1006 produced by the aragonite-to-calcite transformation in speleothems and implications for
1007 paleoclimate reconstructions. *Sedimentary Geology*, 309, 1–14.
1008 <https://doi.org/10.1016/j.sedgeo.2014.05.007>
- 1009